공학박사학위논문

외벽청소로봇을 위한 외란 관측기 기반의 힘 추종 적응형 임피던스 제어기 개발

Force Tracking Adaptive Impedance Controller Based on Disturbance Observer for Building Cleaning Robot

2017년 8월

서울대학교 대학원

기계항공공학부

김 태 균

Abstract

As a lot of high-rise buildings have been recently constructed, demand of systematic and regular operations for their maintenances/inspections has been increasing. Among those operations, wall-cleaning is the most popular and frequently required task.

Unfortunately, since most of wall-cleanings are performed by human operators using ropes or lifts, there is always a possibility of unexpected accidents. These accidents can be the result of workers' carelessness or undesired disturbances like winds and obstacles on walls. Therefore many researches have been going on to replace human workers by robots, developing various types of mobile platforms that can clean up the wall of building perfectly and safely.

This paper presents a modular wall cleaning robot that can be applied to various building shapes and can extend its operating function. The wall-climbing platform can climb up/down various types of walls with the help of the rope ascender and two propeller thrusters. And the cleaning unit can be easily attached and detached through the modular coupling part. Two types of cleaning units have been developed, a dry type cleaning unit and a semi-wet type cleaning unit, which can be replaced according to the types of the surface and the level of pollutant. The cleaning unit has two degrees of freedom on the perpendicular plane to the climbing direction. And the cleaning unit can adjust angle and distance to the wall by ball screw mechanism.

In order to maintain the constant cleaning performance, a force tracking control algorithm is applied. Therefore, a sensor measuring the reaction force is mounted on both ends of the cleaning unit.

The force control of the cleaning unit uses impedance control. Overall control system consists of position-based force tracking impedance controller, disturbance observer and sliding mode controller. The objective of these controllers is to compensate the disturbance, caused by change of distance between the climbing robot platform and the wall, rotation of the cleaning unit brush and the system parameter error. The disturbance observer compensation control input is calculated from the difference of desired force and actual force based on the interaction dynamic model between the cleaning unit and the surrounding condition. And the sliding mode control compensates the disturbance from mismatched uncertainties.

The stability analysis of overall control system is derived and the performance analysis of the controller is carried out through simulations. The performance and stability of the proposed controller is verified with experiments in the test bench reflecting the actual field condition.

Keywords: wall climbing robot, modular cleaning unit, modular manipulator, impedance control, disturbance observer, sliding mode control

Student Number: 2011-20700

Contents

List of the Tables

List of the Figures

Chapter 1

Introduction

1.1 Motivation

As a lot of high-rise buildings have been recently constructed, there has been an increasing demand for systematic and regular operations for their maintenances/inspections and among those operations, a wall-cleaning has been frequently carried out for cleanliness of buildings [1-6]. Unfortunately, since most of wall-cleaning are performed by a human operators using a rope or a lift, there is always a possibility that unexpected accident may occur by his/her carelessness or undesired disturbances like winds and obstacles on walls. From this viewpoint, it is not surprising that many researches have been carried out to develop various types of mobile platforms that can clean up the wall of building perfectly and safely. Some of wall cleaning robots are introduced in next chapter.

1.2 Previous research

Up to now, such devices as a crane on the top of building or built-in rail on the wall of building have been widely adopted for wall-climbing of mobile platforms, which can ensure that the locomotion of wall-cleaning platform is not be affected by the smoothness, profile or cleanliness of walls of buildings [7]. For examples, by using a crane on the top of building, TITO 500 can move in vertical and horizontal directions along a wall of building. While an industrial fan is used to keep in good contact with the wall of building, wheels are installed inside TITO 500 as a damper to prevent undesired collision with the wall of building. At the cleaning speed of 25 m^2/min, TITO 500 cleans up the wall of building by using a rotating brush [8]. Similar to the locomotion of TITO 500, SIRIUSc uses the gantry on the top of building and vacuum suckers are additionally adopted to ensure good adhesion against irregular surfaces. SIRIUSc employs inner/outer sliding modules to move quickly and efficiently along the wall of building and furthermore, the inner modules can rotate around a fixed point to compensate for undesired drift of robot caused by wind, etc. Although the maximum cleaning speed (120 $m^2/hour$) of SIRIUSc is relatively slower than that of TITO 500, it cleans up the wall of building more efficiently by reusing water [9]. Sky-Cleaner 3 can move vertically on a wall by the rope from the following unit on the top of building and also, overcome obstacles by virtue of the suction cup. It can cleans the wall by simultaneously spraying the compressed air and the water provided by the supporting vehicle on the ground [10].

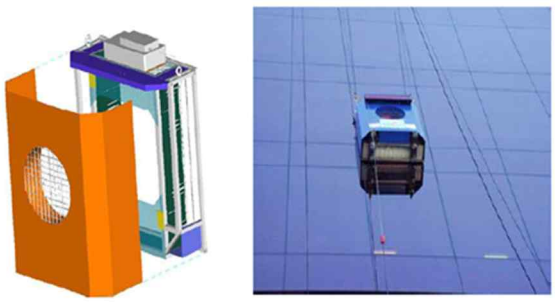

Fig. 1. 1 TITO 500, Industrial Automation Institute, Spain [8]

Fig. 1. 2 SIRIUSc, Fraunhofer Institute for Factory Operation and Automation, Germany [9]

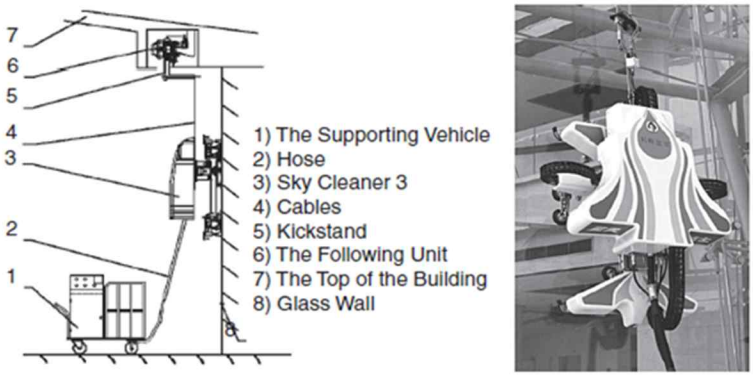

Fig. 1. 3 Sky cleaner 3, University of Hamburg, Germany [10]

The cleaning speed (125 $m^2/hour$) of Sky-Cleaner 3 is similar to that of SIRIUSc but still slower than TITO 500. Complicated control strategies for various pneumatic systems used in X, Y and Z cylinders, brush cylinders and vacuum suckers are inevitably required to ensure desired cleaning performance. Similarly, CAFÉ utilizes the existing carrier system on the building roof and pneumatic actuators to safely move in vertical and horizontal directions along a wall of building. Equipped with the water recycling system, CAFÉ cleans up the wall by using the brush and water in the semi-automatic manner by a human operator. Since CAFÉ uses wheels to move on the wall so that it has the limited capability of overcoming obstacles of 10 mm in height and seems suitable for limited area of building (less than 7000 m^2). The cleaning speed of CAFÉ is 200 $m^2/hour$ [7].

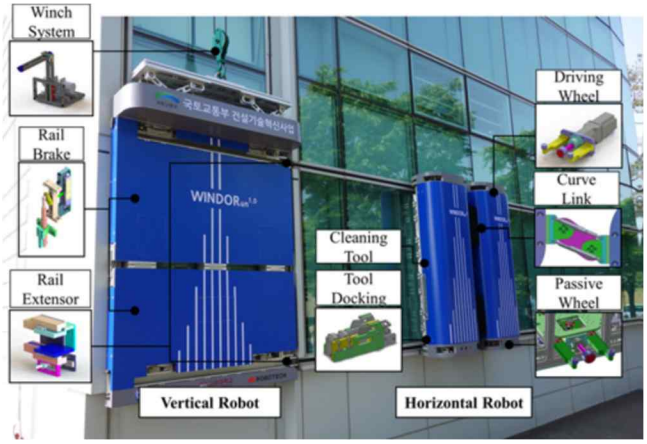

Fig. 1. 4 Building façade maintenance robot, Hanyang University, Korea [11,12]

The building façade maintenance robot (BFMR) can move along the surface of building by using the built-in rails. With the help of the squeeze module equipped with the suction motor, the BFMR enables not only to reuse the water but also to prevent the water from scattering [11, 12]. However, since the built-in rails are indispensable to the climbing operation of BFMR, the cost is inevitably expensive and furthermore, the obstacle-overcoming capability of BFMR is limited. In fact, even though some of previous wall-cleaning systems have acceptable climbing abilities, expensive cost of such devices as cranes and built-in rails still becomes a huge hurdle to their practical uses. For more information on climbing robots, please refer to [13], where the locomotion types of climbing robots and their adhesion principles are well explained and especially, the design aspects for an inspection robot for concrete buildings are in details discussed.

1.3 Objective and scope

This paper represents the new wall cleaning robot which is consists of wall climbing platform and modular cleaning units. The wall-climbing platform can climb up/down various types of walls with the help of the rope ascender and two propeller thrusters. The modular cleaning unit is attached to the wall climbing platform to carry out the cleaning work. And the modular cleaning unit has the parallel link structure of 2-degree of freedom, so the cleaning unit can adjust the distance as well as the contact angle between the unit and a wall. In order to maintain optimal cleaning performance, the working conditions of the cleaning unit are optimized using the Taguchi Method.

Challenging problem of proposed cleaning unit is to keep the constant contact force even if the distance between the actual wall and the robot platform continuously changes and the disturbances exists. The cleaning unit includes a compliance structure at the end of the manipulator and performs repetitive tasks during cleaning work. Due to the complexity of the compliance structure, it is difficult to derive an accurate dynamics equation. And additional sensors are required to consider the dynamic coupling with the wall climbing platform.

Therefore, force tracking control algorithms are developed that can follow the target contact force by measuring only reaction force without additional sensor. The purpose of this controller is to maintain a constant range of force even if disturbances is applied to the cleaning unit. Disturbance includes low frequency disturbances due to distance and angle change between outer wall and robot platform and high frequency disturbances due to rotation of brush.

The control algorithm consists of a force tracking algorithm and a disturbance compensation algorithm. The force tracking algorithm aims to follow the desired force with only loadcell measurements without knowledge of the dynamics of the robot platform and the cleaning unit. And the disturbance compensation algorithm can reject the disturbance to maintain a reaction force within a predetermined bound. The performance of the proposed

controller is demonstrated on a test bench.

The rest of this paper is organized as follows. In Section 2, the kinematic structures and operating principles of proposed climbing platform and cleaning units are explained. And Section 2 presents the optimization of design parameters for operating conditions of cleaning units through the Taguchi method in order to maximize its cleaning performance. In section 3, the kinematics model and the dynamics model of the modular cleaning unit is derived. In Section 4, force tracking algorithms are developed. The force tracking algorithms consists of the position-based impedance control for force tracking and disturbance observer and sliding mode control for disturbance compensation. In Section 5, simulations and experiments demonstrate the performance of the controller. Concluding remarks are presented in Section 6.

Chapter 2

Development of ROPE RIDE

2.1 ROPE RIDE(wall cleaning robot) concept

The proposed mechanism for cleaning a wall of building consists of a wall-climbing platform and two types of modularized cleaning units. The wall-climbing platform can climb up/down various types of walls with the help of the rope ascender and two propeller thrusters. Since the cleaning units are designed in modular manner, they can be easily connected with the wall-climbing platform and also, the applications of proposed wall-climbing platform can be extended from wall-cleaning to wall-painting and inspection, etc. While the dry type cleaning unit cleans up contaminants on a wall by rotating only a brush, the semi-dry type cleaning unit removes solidified contaminants on a wall by vibrating the diatomite pad. The detailed structures and working principles of wall-climbing platform and cleaning units are discussed in the following sections.

.

2.2 Mechanical design

2.2.1 Wall-climbing platform

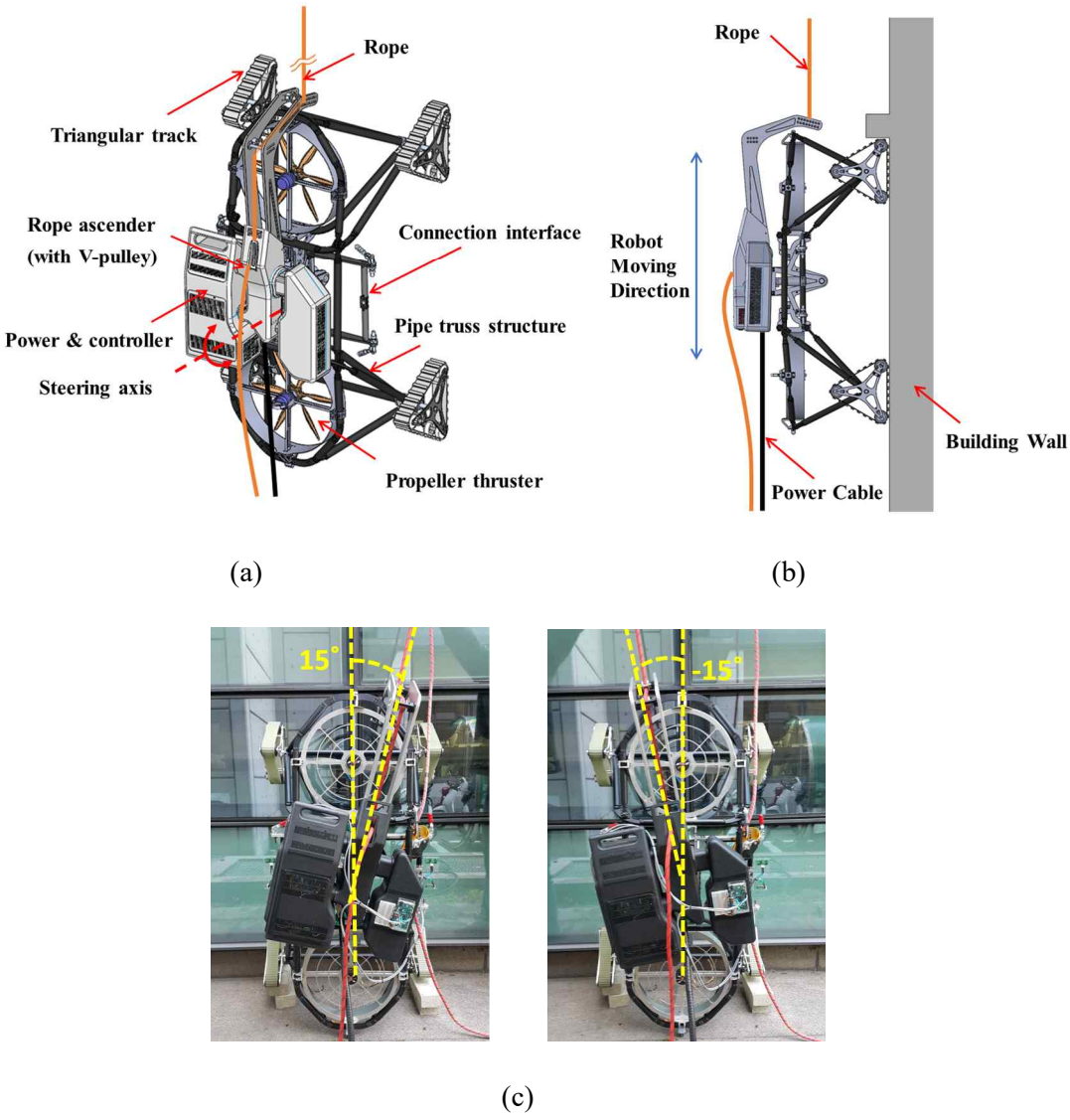

(a) (b)

(c)

Fig. 2. 1 (a) Overall structure, (b) side view of proposed wall-climbing platform and (c) its steering ability of ±15˚ with respect to the rope

Fig. 2.1(a) and (b) show the overall structure and side view of proposed wall-climbing platform which consists of the rope ascender, two propeller thrusters, steering motor and four triangular tracks. The V-type pulley is used in the rope ascender so that it holds the rope due to the self-weight of platform and winds/releases the rope by rotating a motor to move up/down the proposed wall-climbing platform. The main body of proposed wall-climbing platform is composed of the upper and lower bodies, which connected with each other by the steering axis. With the help of steering axis, the lower body can rotate around ±15˚ with respect to the rope as shown in Fig. 2.1(c). While the upper body of platform is equipped with the rope ascender, the steering motor and the connection interface for various types of units, its lower body is equipped with propeller thrusters and triangular tracks. As shown in Fig. 2.1(a), the proposed wall-climbing platform is constructed on the basis of the pipe truss structure in order to ensure its strength as well as lightness so that its weight can be significantly reduced to 37 kg. By virtue of the rope ascender of its upper body, the proposed wall-climbing platform climbs up and down various types of walls of buildings, where the rope can be strongly fixed. Four triangular tracks are designed to move on the wall and rotate if necessary to overcome an obstacle of less than 100 mm in height in combination with two propeller thrusters. Through the experiments designed by the Taguchi method, each propeller thruster is optimally built not only to maximize its thrusting force but also to minimize the resulting noise with maintaining the constant contact force between a wall-cleaning unit and a wall.

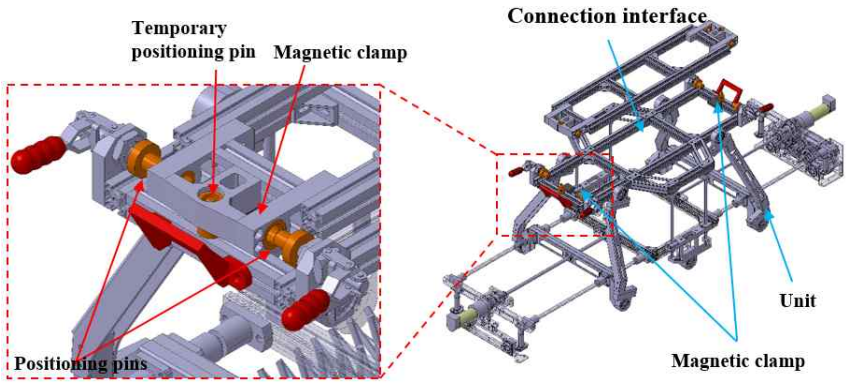

Fig. 2. 2 Concept of modularized connection interface using magnetic clamp

The modularized connection interface with various types of units is installed at the upper body of proposed climbing platform as shown in Fig. 2. 2 In order to connect the cleaning unit with the proposed climbing platform, the positioning pin at both ends of cleaning unit is first connected with the magnetic clamps of climbing platform and then, the positioning pins of climbing platform are tightly connected with the bushes at the edges of cleaning units.

2.2.2 Modular cleaning unit

The schematic diagram of dry type wall-cleaning unit is shown in Fig. 2. 3 The dry type wall-cleaning unit consists of a modularized connection interface, a roller brush for cleaning, two ball-screw mechanism adjusting distance as well as contact angle and infrared proximity sensors for measuring distance and load cells for measuring contact forces, respectively. The modularized connection interface makes it easy for a human operator to attach/detach the dry type wall-cleaning unit to the wall-climbing platform by using a magnetic clamp that can maximally support a payload of 20 kg. Compared to the previous wall-cleaning unit, the weight of dry type wall-cleaning unit is reduced from 20 kg to 16 kg [14, 15]. While the previous wall-cleaning unit can adjust only the distance between the unit and a wall along the vertical direction, the dry type wall-cleaning unit can adjust the distance as well as the contact angle between the unit and a wall. As shown in Fig. 2. 4(a) and 2. 4(b), the position of ball-screw nuts connecting the cleaning unit with the modularized connection interface can be controlled appropriately by rotating two ball-screw mechanisms. For examples, if two ball-screw mechanisms rotate at the same rotating speeds, the distance between the cleaning unit and a wall is adjusted and if they rotate at the different rotating speeds, the contact angle between them is adjusted. As a result, the stroke and contact angle of dry type wall-cleaning unit can be maximally up to 150 mm and ±13˚, respectively, which enables the proposed wall-climbing platform to not only overcome different types of obstacles on walls but also ensure the excellent contact ability of wall-cleaning units irrespective of various shapes of walls. It is obvious that in order to effectively remove contaminants from a wall, the contact force between the cleaning unit and a wall must be kept higher than a certain level. Therefore, to measure the contact force between the cleaning unit and a wall, two load cells are installed

at the both ends of cleaning unit. Also, four infrared proximity sensors are installed at the edges of cleaning unit in order to precisely measure the distance between the cleaning unit and a wall, which can help not only implement the position-based impedance control (PIC) strategy but also prevent the wall-cleaning unit from colliding with the obstacles on a wall [15]. Two roller brushes are made of PP material which has good restoration as well as sufficient sharpness to remove the contaminants on a wall. Note that as shown in Fig. 2. 4(c), the proposed cleaning unit has the contact ability required for cleaning the curved wall of larger than a certain curvature because the contact angles of left and right-side links can be continuously adjusted through the ball-screw mechanisms. In fact, from the geometric relation in Fig. 2. 4(d), when the cleaning unit meets the curved wall tangentially at the maximum contact angle (=13˚), the minimum radius of curvature is about 2890 mm, which implies that the proposed cleaning unit has the sufficient contact ability against the curved walls of general high-rise buildings because their radius of curvatures are typically larger than 2890 mm.

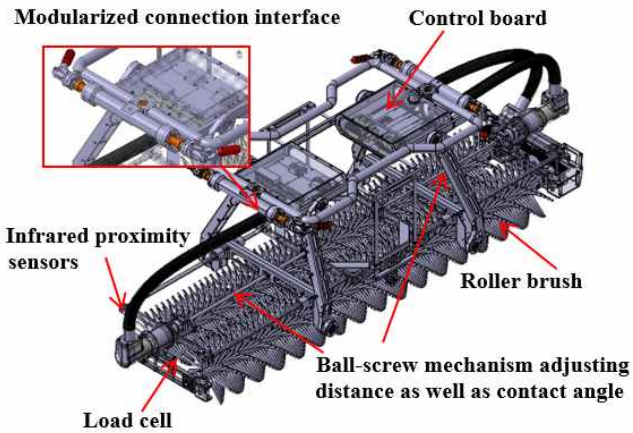

Fig. 2. 3 Schematic diagram of dry type wall-cleaning unit

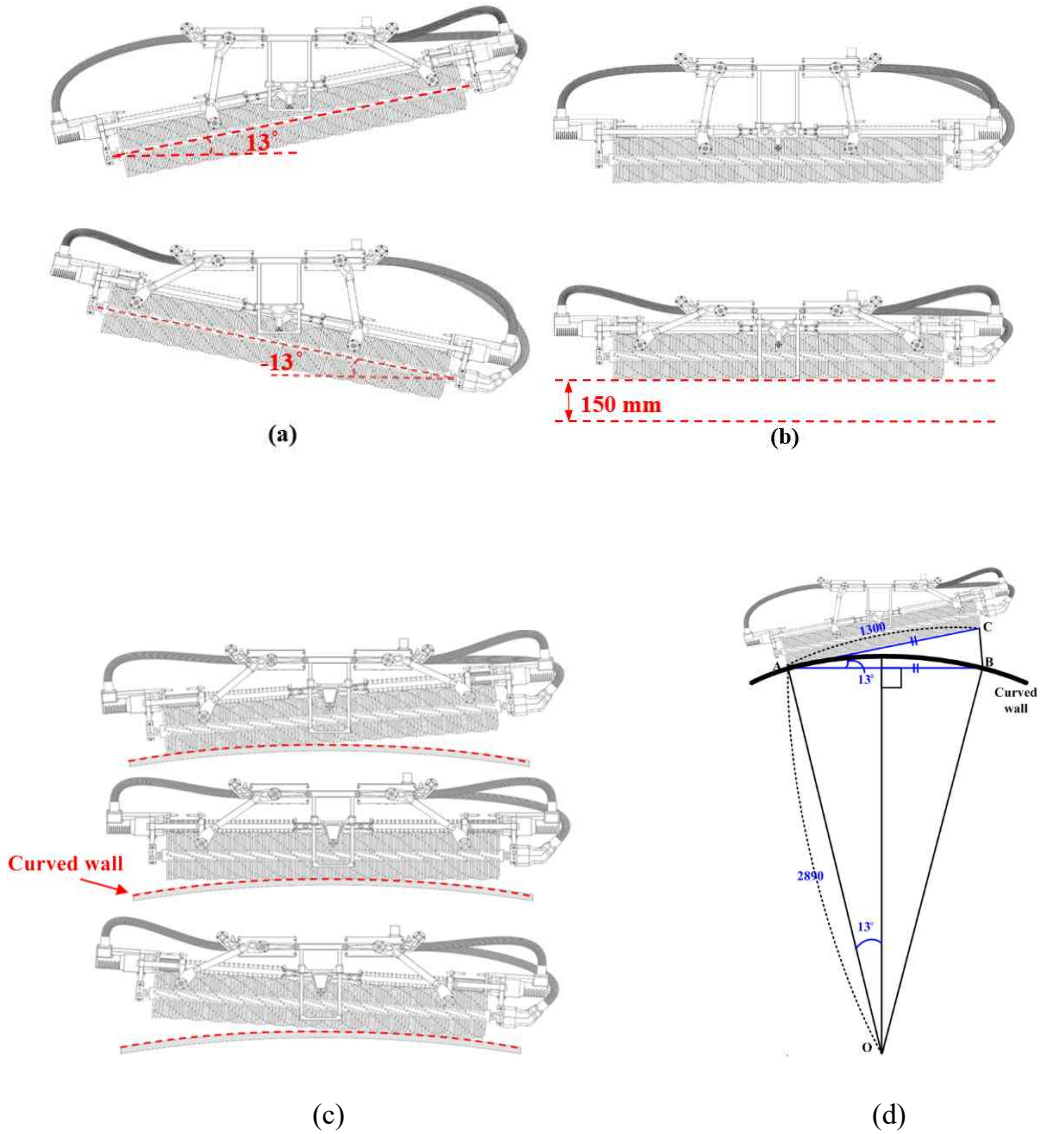

Fig. 2. 4 (a) Adjustment of contact angle, (b) distance between the wall-cleaning unit and a wall, (c) schematics of cleaning the curved wall and (d) minimum radius of curvature at the maximum contact angle

Compared to the dry type wall-cleaning unit using only the roller brushes without waters, the semi-dry type wall-cleaning unit is proposed to effectively remove solidified contaminants on a wall so that it is additionally equipped with the diatomite supply unit and the vibration pad instead of the roller brush as shown in Fig. 2. 5. It is known that the advantages of cleaning method using the diatomite is to not only use no water while cleaning but also clean up a wider area of wall by using one wiper [14]. In order to ensure the sufficient contact frequency between the pad and a wall, the vibration mechanism is used, which attaches several eccentric masses to the end of high-speed rotating motor in order to generate several vibrations of different frequencies at the same time. In addition, the ball roller is used to prevent the deformation of vibration pads and in order to prevent the vibration generated by the vibration mechanism from being transmitted to the wall-climbing platform, the sponge absorber is installed between the vibration mechanism and the pad. Recall that both types of wall-cleaning units do not use water for cleaning the wall. Of course, if water is used for cleaning, the cleaning performance may be improved but it is worthwhile to note that additional device is required in order to supply water for high-rise building, which inevitably increases the weight of climbing platform and furthermore, the secondary contamination of cleaned walls may occur if used water cannot be completely recirculated. So we have tried to develop a wall-cleaning unit without using water.

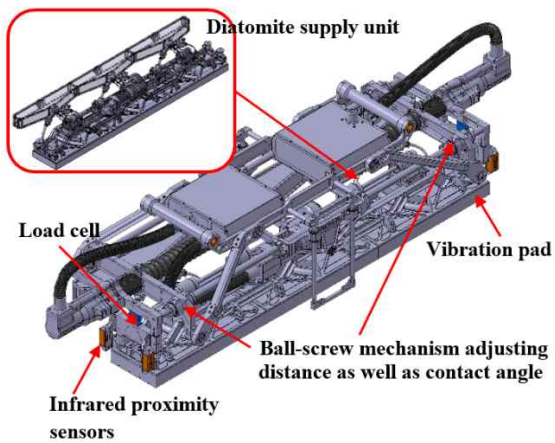

Fig. 2. 5 Schematic diagram of semi-dry type wall-cleaning unit

2.2.3 Hardware architectures of wall-climbing platform and cleaning unit

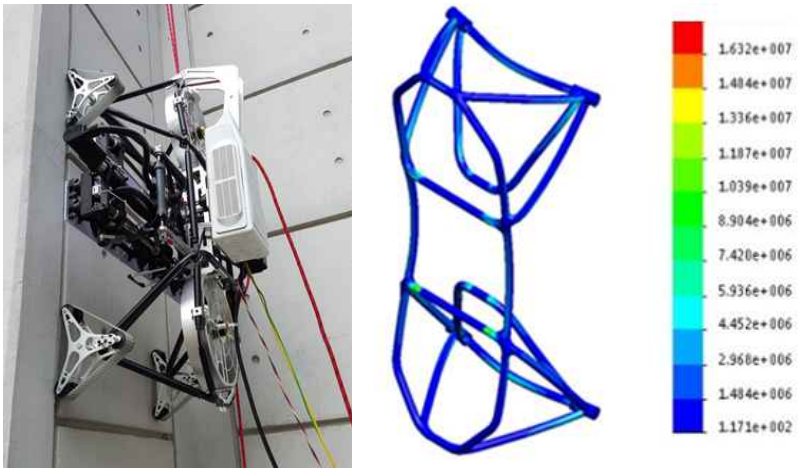

(a) (b)

Fig. 2. 6 (a) Prototype of wall-climbing platform equipped with the semi-dry type cleaning unit and (b) finite element analysis of stress distribution on frame for wall-climbing platform

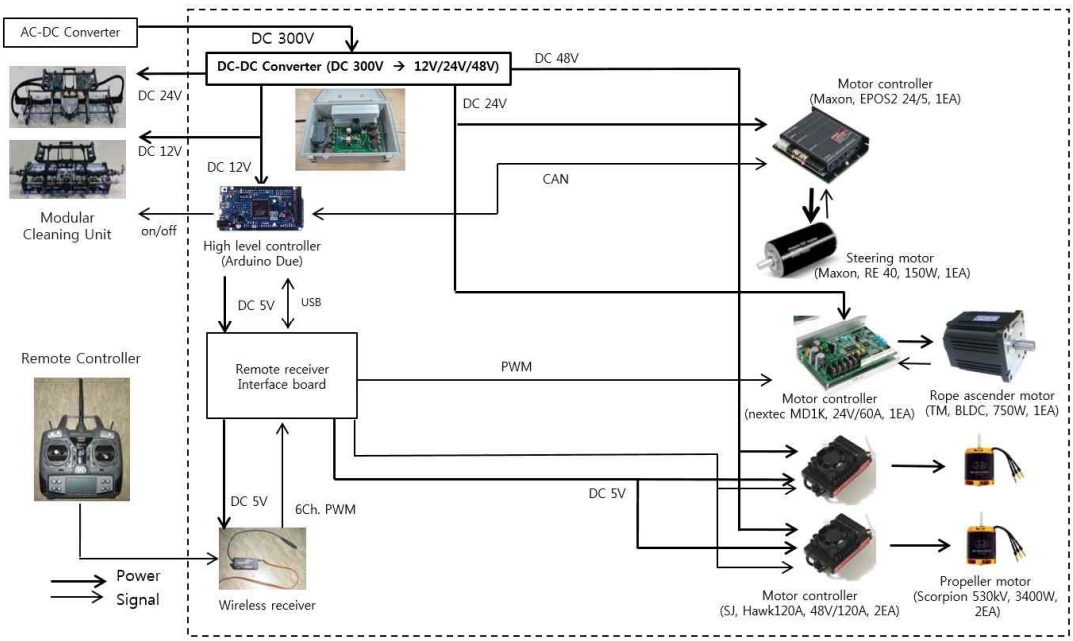

Fig. 2. 7 Hardware architecture of wall-climbing platform

The prototype of the wall-climbing platform equipped with the semi-dry type wall cleaning unit is shown in Fig. 2. 6(a). The maximum payload and climbing speed of proposed wall-climbing platform are 18 kg and 0.148 m/sec, respectively. The proposed wall-climbing platform is constructed upon the pipe truss frame in order to not only reduce the overall weight of climbing platform but also increase the operator's convenience in adjusting the position of climbing platform at the initial operation, etc. The hollow pipe of 4 mm in thickness is made of AL 6061-T6 and the external case is made of plastic resin by using a 3D printer, respectively. The finite element analysis in Fig. 2. 6(b) shows that the maximum stress acting on the wall-climbing platform is 17.8 MN/m2, which is quite smaller than the maximum tensile stress of AL 6061-T6.

The hardware architecture of the wall-climbing platform is in details shown in Fig. 2. 7. The proposed wall-climbing platform is controlled wirelessly by a human operator using a remote controller, who can give commands to control the RPM of thrusting propeller, climbing up/down velocities of rope ascender, tilting angle of steering mechanism and on/off operation of wall-cleaning unit. As for the power supply, the external AC-DC converter is adopted to convert 220V AC to 300V DC on the ground in order to reduce the weights of wire and platform. Then, 300V DC is supplied to the proposed climbing platform via the black wire in Fig. 2. 6(a) and again converted to 12V/24V/48V DC through the DC-DC converter installed in the proposed climbing platform for driving motors, motor drives and cleaning units. The Arduino Due board is adopted for steering of wall-climbing platform and on/off operation of wall-cleaning unit while the commands for rope ascending motors and propeller thrusting motors are directly given from the wireless receiver to the drives via the remote receiver interface board.

Fig. 2. 8 shows the hardware architecture of wall-cleaning unit. 12V and 24V DCs from the DC-DC converters of wall-climbing platform are transmitted to the high level control board (NI, sbRIO) and three motor drives (Maxon, EPOS2 70/10), respectively. The on/off signal is given from Arduino Due to sbRIO for activating the control algorithm of cleaning unit so that if the off signal is given, the wall-cleaning unit is raised up from a wall but if the

on signal is given, the wall-cleaning unit starts to clean a wall according to the control algorithm to maintain the contact force constantly. In order to effectively avoid obstacles in the longitudinal direction while cleaning up a wall, four infrared sensors (SHARP) are used to measure the distance from the wall-cleaning unit to obstacles. Two load cells (CASKOREA, DBCM20) are used to measure the contact force between the cleaning unit and a wall with the aim of maintaining the contact force constantly. The velocity and position commands between the high level control board and motor drives are transmitted through the CAN. The weights of dry type and semi-dry type cleaning units are 15.95 kg and 16.65 kg, respectively and the distance and contact angle between the rotating brush or vibrating pad and a wall can be adjusted up to 150 mm and and ±13˚ as shown in Fig. 2.4.

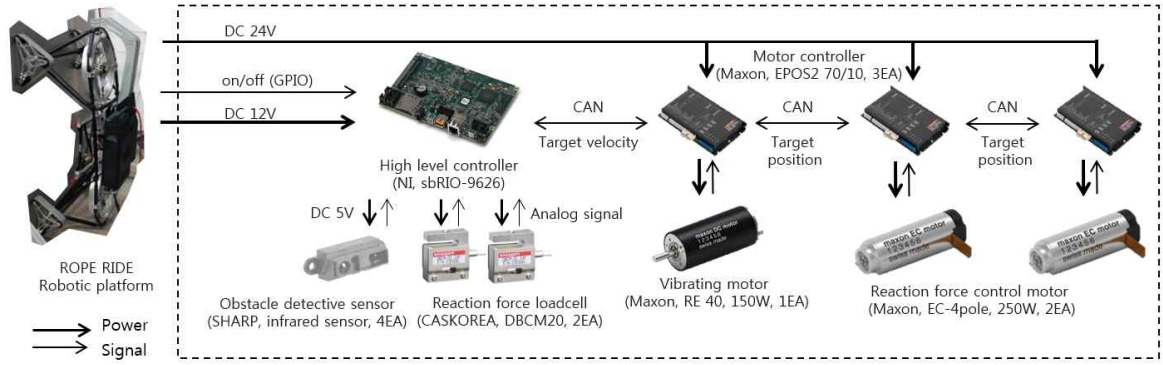

Fig. 2. 8 Hardware architecture of wall-cleaning unit

2.3 Optimization of operating conditions for wall-cleaning unit

It is quite important to ensure a consistent cleaning performance of proposed wall-cleaning unit against contaminated walls. First, in order to evaluate the cleaning performance of wall-cleaning unit properly, the light transmissivity of cleaned wall is chosen as the performance criterion in this study and is measured by a window energy profiler which does not need additional light for measurement. Also, in order to find out the optimal operating conditions for the wall-cleaning unit, the experimental setup is newly designed and

manufactured to implement various operating conditions on type of brush, contact force, rotating speed of brush and moving speed of wall-climbing platform. Figs. 2. 9(a) and 2. 9(b) show the schematic diagram and real photograph of experimental setup, respectively. As shown in Fig. 2. 9(a), a glass can be easily moved up/down by the human operator with the help of the pulley, which makes it possible to adjust the moving speed of glass. The metronome is used to measure the time period while the human operator moves up/down the glass by the pulley. Then, the moving speed of glass can be obtained by dividing its moving distance with the time period measured by the metronome. The guide rail is installed in the middle of experimental setup, which can move the brush of cleaning unit forward/backward precisely by a car jack with the aim of controlling the contact force between a glass and the brush of cleaning unit. The push-pull gauge is installed as shown in Fig. 2. 9(a) to measure this contact force between a glass and the brush. Two brushes are used for wall-cleaning, which are connected to the motors via bevel gears.

In order to streamline the optimization of operating conditions for the wall-cleaning unit via the Taguchi method, the preliminary experiments are first performed to compare the cleaning performances of different types of brushes. Four types of brushes are considered for experiments: general type, spiral type, V-type and high density brushes. The experiments are twice conducted for each brush by using the experimental setup in Fig. 2. 9, where the contact forces are set to be 20 N and 40 N with the rotating speed of brush of 100 RPM. In order to reproduce the contaminated glass, the red clay combined with water is spread on a glass and dried. The experimental results are summarized in Table A3 of Appendix. As confirmed in Table A3, the cleaning performance of cleaning unit using the spiral brush is most excellent in comparison to those using other types of brushes. Second, the cleaning performances of cleaning unit using the V-type brush is acceptable but it is observed that its cleaning performance may be significantly deteriorated when the contact force is slightly changed. On the other hand, the cleaning performance of cleaning unit using the high-density type brush is worst because its brush pattern remains on the glass after cleaning. Therefore, the spiral brush is chosen for the experiments to optimize the operating conditions for the wall-cleaning unit.

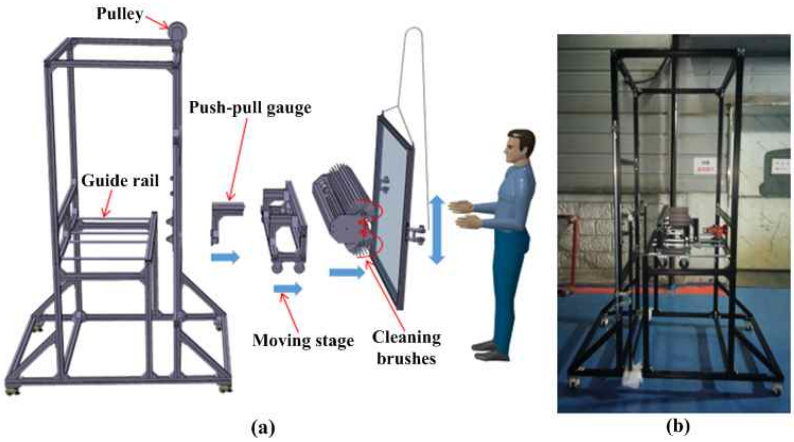

Fig. 2. 9 (a) Schematic diagram and (b) real photograph of experimental setup for reproducing different operating conditions for wall-cleaning unit

In this study, in order to find out the optimal condition for the wall-cleaning unit to maximize the light transmissivity, the Taguchi method is adopted, where the rotating speed of brush (A), the contact force between a wall and brush (B) and the moving speed of glass (C) are chosen as control factors. It is worthwhile to note that the cleaning performance is highly related with the light transmissivity of cleaned glass so that as the light transmissivity becomes higher, more excellent cleaning performance can be ensured. Therefore, this optimization can be considered as the-larger-the-better case. Therefore, the following S/N ratio is used for optimization of operating conditions:

$$S/N = -10\log_{10}\left\{\sum_{k=1}^{l}\frac{1}{(y_{L,after})_k^2}\right\} \quad (2.\ 1)$$

where l and $y_{L,after}$ denote the number of repetition in experiments and the light transmissivities of glass after cleaning, respectively. The levels of all control factors are chosen to be three and their corresponding values are given in Table 2.1. Recall that high rotating speed of brush or high contact force between a glass and brushes may cause

undesired vibrations or disturbances to the climbing platform, which will be an obstacle to the mobile stability of wall-climbing platform. From this respect, the values for these control factors are carefully chosen through the preliminary experiments. In order to ensure the reliability of measurement, the light transmissivity of glass is measured at 5 points of left/right side of glass after cleaning so that in this study, the number of repetition l=10. Since there are 3 control factors of three levels, the experiments are performed with the orthogonal array $L_9(3^4)$. The measured light transmissivity and resulting average S/N ratios are summarized in Table 2.2.

Table 2. 1 Design parameters for optimization of operating conditions for wall-cleaning unit

		Level 1	Level 2	Level 3
A	Rotating speed of brush (RPM)	100	200	300
B	Contact force (N)	20	30	40
C	Moving speed of glass (m/s)	0.1	0.13	0.16

Table 2. 2 Cost functions and S/N ratios in the optimization of operating conditions for wall-cleaning unit

	Rotating speed of brush (RPM)	Contact force (N)	Moving speed of glass (m/s)	Light transmissivity before cleaning		Light transmissivity after cleaning		S/N
1	1	1	1	74	75	83	81	38.00
				70	75	81	72	
				73	71	85	83	

				76	65	83	75	
				71	69	81	74	
2	1	2	2	77	72	85	82	38.42
				79	77	84	83	
				74	74	85	85	
				74	78	84	82	
				63	74	83	81	
3	1	3	3	79	73	84	83	38.29
				71	64	83	81	
				67	76	81	83	
				73	65	84	82	
				71	58	80	81	
4	2	1	2	59	71	84	84	38.26
				75	68	84	79	
				75	70	84	83	
				71	65	85	77	
				77	58	83	77	
5	2	2	3	72	72	84	83	38.41
				77	75	85	81	
				70	74	84	83	
				71	76	84	83	
				71	73	83	83	
6	2	3	1	75	68	85	86	38.58
				74	69	86	86	
				74	72	83	84	
				72	68	85	85	
				76	71	85	84	
				69	76	82	81	

7	3	1	3	75	71	83	72	37.97
				63	77	83	83	
				73	71	82	77	
				71	64	83	70	
8	3	2	1	74	67	84	83	38.48
				71	71	85	83	
				65	67	84	83	
				72	71	84	85	
				53	65	85	84	
9	3	3	2	73	68	85	86	38.48
				71	68	82	86	
				69	72	82	83	
				69	78	84	86	
				66	54	82	84	

Fig. 2. 10 Average S/N ratios with respect to control factors for optimization of operating conditions for wall-cleaning unit

Fig. 2. 10 shows the average S/N ratios with respect to control factors for optimization of operating conditions for wall-cleaning unit. As shown in Fig. 2. 10, the optimal levels of rotating speed of brush and contact forces are 1 and 3 while the level of moving speed of glass is 1, which may be quite reasonable because as the rotating speed of brush and the contact force increase but the moving speed of glass decreases, the contaminants on glass can be removed easily. Since the difference between average S/N ratios at contact forces of level 2 and 3 is too small (=0.02) and negligible, the contact force for wall-cleaning unit is set to be 30 N in order not to disturb the mobile stability of wall-climbing platform. Also, since the maximum target climbing speed of wall-climbing platform is 0.15 m/s, the moving speed of wall-climbing platform is fixed to be 0.1 m/s. Fig. 2. 11 compares the contaminated glass before cleaning with the glass cleaned by brushes under operating conditions obtained in the optimization. As confirmed in Fig. 2. 11, the most of contaminants on the cleaned glass are removed considerably so that the S/N ratio in Eq. (3) is up to 38.71.

Fig. 2. 11 Comparison of contaminated glass (before cleaning) and cleaned glass

2.4 Experiments

Fig. 2. 12 describes the detailed operation sequence of proposed wall-climbing platform and the schematics of wall-climbing platform cleaning the wall of building along the lane. The operation sequence can be summarized as follows: First, the rope is fixed to one of several solid structures on the top of building (called as the fixing points in this paper) by the human operator and let down to the ground. Then, the rope is installed to the proposed climbing platform via the ascender. It is noted that the proposed climbing platform is the semi-automated one so that the human operator is required to control the climbing platform and cleaning units properly by adjusting the rotating speeds of propellers, the ascending/descending speed of rope and turning on/off the cleaning units, etc when the wall-climbing platform goes up/down along the lane on the wall of building. After completing the cleaning of wall along the lane, the rope is moved and fixed to the next fixing point on the top of building by the human operator. Of course, the wall-climbing platform is moved to the next position at the same time. This procedure will be repeated before cleaning all the lanes on the wall of building.

Fig. 2. 13 shows the snapshots of the proposed wall-climbing platform equipped with the dry type cleaning unit while climbing up a wall of building at the speed of 0.148 m/s, whose concrete exterior consists of obstacles like steel thresholds. From Fig. 2. 13, the proposed wall-climbing platform enables to climb a wall of building with overcoming the obstacles on a wall effectively. Also, as shown in Figs. 2. 13(5) and 2. 13(6), the proposed wall-climbing platform can overcome two obstacles of different heights at the same time. In this case, the wall-cleaning unit is raised up without cleaning a wall. For more details, please refer to the multimedia file whose title is ‘climbing of wall climbing platform’.

Figs. 2.14(a) and 2.14(b) show the snapshots of the proposed wall-climbing platform equipped with the dry type and semi-dry type wall-cleaning units with cleaning glasses during its climbing, respectively. In both cases, the wall-cleaning units are automatically raised up to avoid undesired collision with obstacles on a wall. While the wall-climbing platform climbs up a flat wall, the dry type wall cleaning unit cleans up the wall by rotating

brushes and the semi-dry type wall cleaning unit removes the solidified contaminants on the wall by vibrating the diatomite pad on it with keeping in contact with the wall. For more details, please refer to the multimedia files whose titles are ‘cleaning with dry type unit’ and ‘cleaning with semi dry type unit’.

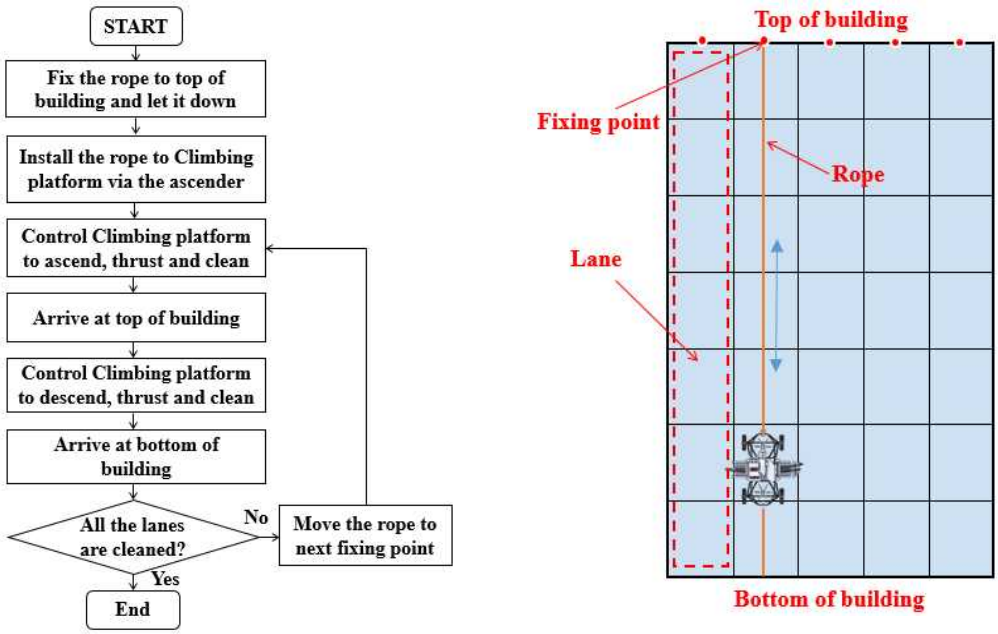

(a) (b)

Fig. 2. 12 (a) Operating sequence of proposed climbing platform and (b) schematic diagram of wall-climbing platform cleaning the wall of building along the lane

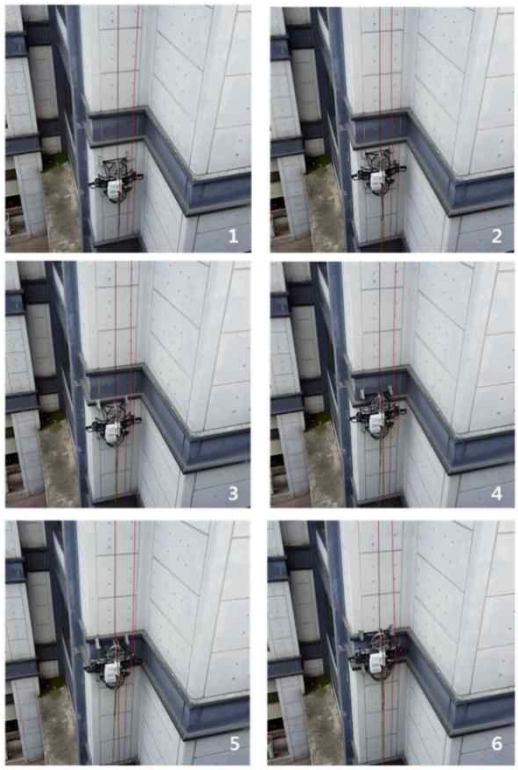

Fig. 2. 13 Snapshots of proposed wall-climbing unit equipped with dry-type cleaning unit climbing up a wall of building

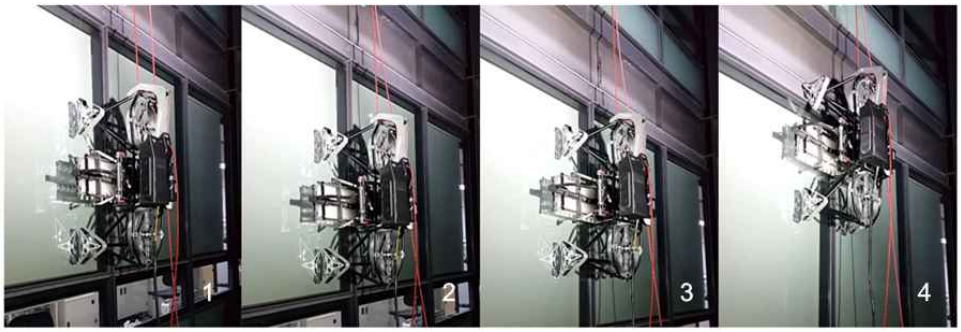

(a)

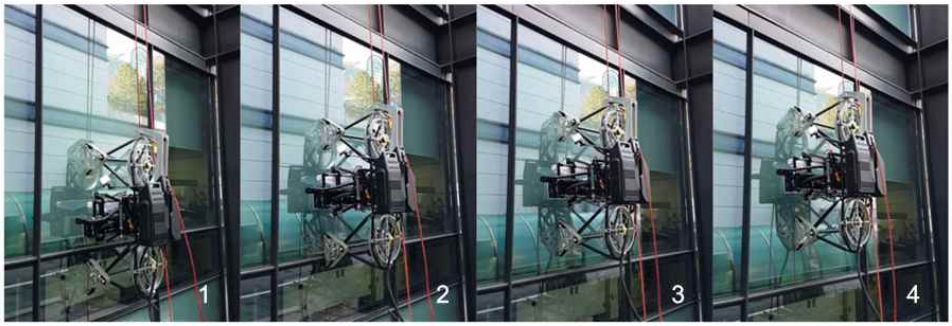

(b)

Fig. 2. 14 Snapshots of proposed wall-climbing unit equipped with (a) the dry type cleaning unit and (b) semi-dry type cleaning unit with cleaning glasses during its climbing

For fair evaluation of the cleaning performance of wall-cleaning unit, the test bench for the wall-cleaning unit is manufactured as shown in Fig. 2. 15. As shown in Fig. 2. 15(a), the wall-cleaning unit is installed in the test bench by using clamp unit and along the vertical axis, the wall-cleaning unit can move up/down at the same speed as the wall-climbing platform climbs up/down a wall. Of course, the distance between the cleaning unit and the wall of test bench can be adjusted along the horizontal direction. Fig. 2. 15(b) explains the cleaning test procedure of wall cleaning unit. After installing the cleaning unit in the test bench as shown in Fig. 2. 15(b)-1, the distance between the cleaning unit and the wall is set

to be a certain value for force tracking via switching position-based impedance control (SPIC) as shown in Fig. 2. 15(b)-2. The cleaning unit cleans up the wall with rotating brushes and moving along the vertical axis as shown in Figs. 2. 15(b)-3 and 4. The test is carried out by using glass specimen in order to evaluate the cleaning performance of cleaning unit as shown in Fig. 2. 15(c), where the rotating speed of brushes and the moving speed of cleaning unit are 120 RPM and 40 mm/s, respectively. The contact force between the cleaning unit and the wall is set to be 30 N. It is noted that the optimal operating conditions for wall-cleaning unit are that the rotating speed of brush and the moving speed of wall cleaning unit are 300 RPM and 0.1 m/s but since the moving speed of cleaning unit in the test bench is limited to 40 mm/s, the rotating speed of brush is accordingly adjusted. Table 2.3 compares the light transmissivities of five contaminated glass specimens with those of cleaned glass specimens. Since the light transmissivity of clean 5 mm tempered glass is 89 %, the criterion for cleaning performance is chosen to be 82 % (up to 91 % of light transmissivity of clean 5 mm tempered glass). As confirmed in Table 2.3, the light transmissivities of cleaned glass specimens are significantly improved by more than 30 % compared to those of contaminated ones so that the light transmissivities of cleaned glass are almost same as initial light transmissivities of original glasses, which proves the cleaning performance of wall-cleaning unit is quite acceptable.

Table 2. 3 Test results of cleaning performance of dry type cleaning unit using test bench

	Light transmissivity of specimen				
	Specimen 1	Specimen 2	Specimen 3	Specimen 4	Specimen 5
Initial	88.9	89.1	89.1	88.9	89.1
After contamination	63.4	55.4	55.4	58.7	61.9
After cleaning	88.9	89.1	89.1	88.9	89.1

(b)

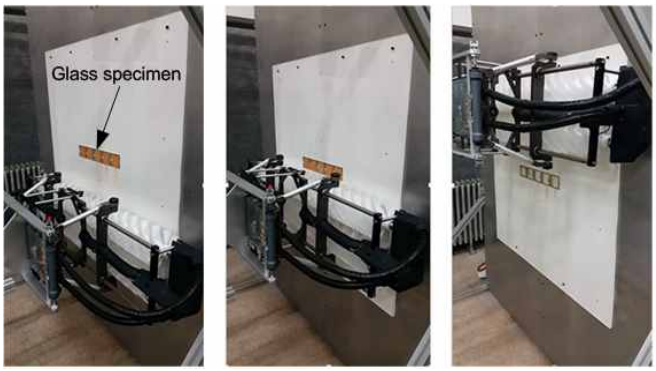

(c)

Fig. 2. 15 Snapshots of (a) test bench for dry type wall cleaning unit, (b) sequential operations of dry type wall cleaning unit and (c) test using glass specimen

Chapter 3

Modeling of modular cleaning unit

3.1 Description of kinematics model

The kinematic model of the cleaning unit is shown in Fig. 3.1. The restraint equation of the cleaning unit link is as follows.

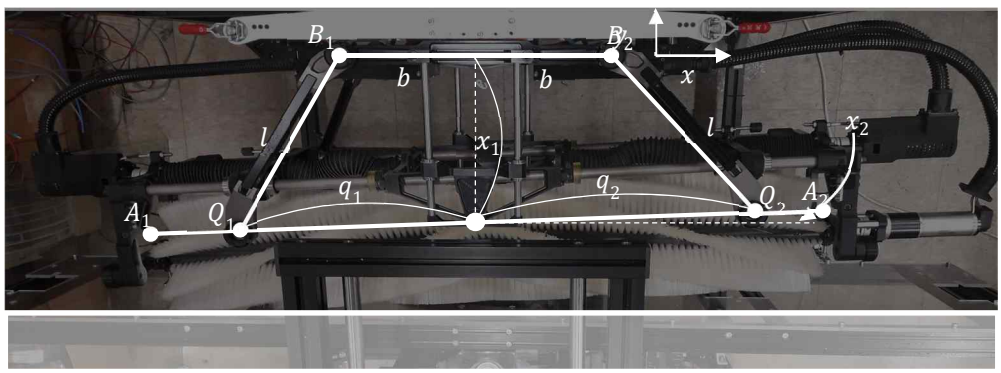

Fig. 3. 1 Kinematic structure of the cleaning unit

$$(x_1 + q_1 sin\ x_2)^2 + (q_1 cos\ x_2 - b)^2 = l^2$$

$$(x_1 - q_2 sin\ x_2)^2 + (-q_2 cos\ x_2 + b)^2 = l^2 \quad (3.1)$$

$$q_1 = \frac{\varphi_1}{2\pi} L\ ,\ q_2 = \frac{\varphi_2}{2\pi} L$$

$\varphi_1,\ \varphi_2$ are the ball screw rotation angle and L is the ball screw lead.

By rearranging the constraint equations

$$x_1{}^2 + 2x_1 q_1 sin\ x_2 - 2bq_1 cos\ x_2 = l^2 - b^2 - q_1{}^2$$

$$x_1{}^2 - 2x_1 q_2 sin\ x_2 - 2bq_2 cos\ x_2 = l^2 - b^2 - q_2{}^2 \quad (3.2)$$

Based on these, inverse kinematics can be obtained as

$$x_2 = \arcsin\frac{h_1 - h_2}{2d}\ , x_1 = \frac{h_1 + h_2}{2}$$

$$q_1 = -(x_1 \sin x_2 - b\cos x_2) + \sqrt{(x_1 \sin x_2 - b\cos x_2)^2 - x_1{}^2 - b^2 + l^2} \quad (3.3)$$

$$q_2 = (x_1 \sin x_2 + b\cos x_2) + \sqrt{(x_1 \sin x_2 + b\cos x_2)^2 - x_1{}^2 - b^2 + l^2}$$

In the case of forward kinematics, there is no analytical solution because the equation for $cos\ x_2$ is 8th order equation. Therefore, the forward kinematics solution using Taylor series expansion is as follows. [16]

From $|x_2| < \frac{\pi}{18}$, $\sin(x_2) \approx x_2$, $\cos(x_2) \approx 1$ (maximum error : -1.5%)

$$\theta_1 = arcsin\ \ \frac{q_1 - b}{l}\ ,\ \ \theta_2 = arcsin\ \ \frac{q_2 - b}{l}$$

$$x_2 = \frac{l\cos(\theta_1) - l\cos(\theta_2)}{q_1 + q_2},\ x_1 = \frac{q_2 l\cos(\theta_1) - q_1 l\cos(\theta_2)}{q_1 + q_2} \quad (3.4)$$

$$h_1 = x_1 + d\sin(x_2),\ h_2 = x_1 - d\sin(x_2)$$

Based on the above equations, the maximum estimation error of forward kinematics is -8.78 mm (-5.28 %).The average estimation error is -0.52 mm and standard deviation is 1.22 mm.

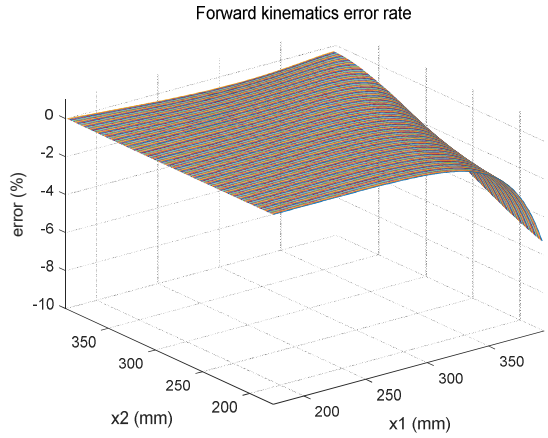

Fig. 3. 2 Estimation error rate of forward kinematics by taylor series expansion

From the constraint equations Jacobian can be obtained as follows.

By multiplying ${J_x}^{-1}$ to both sides of $J_q\dot{\boldsymbol{q}} = J_x\dot{\boldsymbol{x}}$, ${J_x}^{-1}J_q\dot{\boldsymbol{q}} = \dot{\boldsymbol{x}}$ is obtained and it can be expressed as $\boldsymbol{J}\dot{\boldsymbol{q}} = \dot{\boldsymbol{x}}$.

Where, $\dot{\boldsymbol{q}} = \begin{bmatrix} \dot{q_1} \\ \dot{q_2} \end{bmatrix}, \dot{\boldsymbol{x}} = \begin{bmatrix} \dot{x_1} \\ \dot{x_2} \end{bmatrix}$

$$J_x = \begin{bmatrix} x_1 + q_1 \sin x_2 & x_1 q_1 \cos x_2 + b q_1 \sin x_2 \\ x_1 - q_2 \sin x_2 & -x_1 q_2 \cos x_2 + b q_2 \sin x_2 \end{bmatrix} \tag{3.5}$$

$$J_q = \begin{bmatrix} b \cos x_2 & -x_1 \sin x_2 - q_1 & 0 \\ 0 & & b \cos x_2 + x_1 \sin x_2 - q_2 \end{bmatrix} \tag{3.6}$$

$\boldsymbol{J} = {J_x}^{-1}J_q =$

$$\begin{bmatrix} \frac{-q_2(b\sin x_2 - x_1\cos x_2)(b\cos x_2 - q_1 + x_1\sin x_2)}{{x_1}^2\cos x_2(q_1+q_2)+b\sin x_2(q_1x_1-q_2x_1-2q_1q_2\sin^2 x_2)} & \frac{q_1(b\sin x_2 + x_1\cos x_2)(b\cos x_2 - q_2 + x_1\sin x_2)}{{x_1}^2\cos x_2(q_1+q_2)+b\sin x_2(q_1x_1-q_2x_1-2q_1q_2\sin^2 x_2)} \\ \frac{(x_1 - q_2\sin x_2)(b\cos x_2 - q_1 + x_1\sin x_2)}{{x_1}^2\cos x_2(q_1+q_2)+b\sin x_2(q_1x_1-q_2x_1-2q_1q_2\sin^2 x_2)} & \frac{-(x_1 - q_1\sin x_2)(b\cos x_2 - q_2 + x_1\sin x_2)}{{x_1}^2\cos x_2(q_1+q_2)+b\sin x_2(q_1x_1-q_2x_1-2q_1q_2\sin^2 x_2)} \end{bmatrix} \begin{bmatrix} \dot{q_1} \\ \dot{q_2} \end{bmatrix}$$

(3.7)

$$\boldsymbol{J}^{-1} = {J_q}^{-1}J_x = \begin{bmatrix} \frac{x_1 + q_1\sin x_2}{b\cos x_2 - x_1\sin x_2 - q_1} & \frac{x_1q_1\cos x_2 + bq_1\sin x_2}{b\cos x_2 - x_1\sin x_2 - q_1} \\ \frac{x_1 - q_2\sin x_2}{b\cos x_2 + x_1\sin x_2 - q_2} & \frac{-x_1q_2\cos x_2 + bq_2\sin x_2}{b\cos x_2 + x_1\sin x_2 - q_2} \end{bmatrix} \tag{3.8}$$

The acceleration related equations are as follow.

$$\frac{d}{dt}(\boldsymbol{J}\dot{\boldsymbol{q}}) = \frac{d}{dt}\dot{\boldsymbol{x}} \text{ becomes } \dot{\boldsymbol{J}}\dot{\boldsymbol{q}} + \boldsymbol{J}\ddot{\boldsymbol{q}} = \ddot{\boldsymbol{x}} \tag{3.9}$$

Where, $\ddot{\boldsymbol{x}} = \begin{bmatrix} \ddot{x_1} \\ \ddot{x_2} \end{bmatrix}$, $\dot{\boldsymbol{J}} = \dot{J_x^{-1}}J_q + J_x^{-1}\dot{J_q}$,

3.2 Description of dynamics model

Virtual work equations are as follow.

$$J\delta q = \delta x \text{ where } \delta q = \begin{bmatrix} \delta q_1 \\ \delta q_2 \end{bmatrix}, \delta x = \begin{bmatrix} \delta x_1 \\ \delta x_2 \end{bmatrix}$$

According to virtual work principal, the relation between the force (F_1, F_2) acting on the end effector of the cleaning unit and the speed, acceleration $(\dot{q}, \ddot{q})$, and motor torque (τ_1, τ_2).

$$\delta W = \tau_1 \cdot \delta q_1 + \tau_2 \cdot \delta q_2 + (F_1 - m_1\ddot{x_1}) \cdot \delta x_1 + (F_2 - m_2\ddot{x_2}) \cdot \delta x_2 = 0 \tag{3.10}$$

$$= [\tau_1 \quad \tau_2]\begin{bmatrix} \delta q_1 \\ \delta q_2 \end{bmatrix} + \left(\begin{bmatrix} F_1 & 0 \\ 0 & F_2 \end{bmatrix} - \begin{bmatrix} m_1 & 0 \\ 0 & m_2 \end{bmatrix}\begin{bmatrix} \ddot{x_1} \\ \ddot{x_2} \end{bmatrix}\right)\begin{bmatrix} \delta x_1 \\ \delta x_2 \end{bmatrix} = 0$$

$$= \tau\delta q + (F - m\ddot{x})\delta x = 0$$

Where, $\tau = [\tau_1 \quad \tau_2]$, $F = \begin{bmatrix} F_1 & 0 \\ 0 & F_2 \end{bmatrix}$, $m = \begin{bmatrix} m_1 & 0 \\ 0 & m_2 \end{bmatrix}$

$= \tau\delta q + (F - m\ddot{x})J\delta q = (\tau + (F - m\ddot{x})J)\delta q = 0$

From $\tau + (F - m\ddot{x})J = 0$, following equation can be derived.

$$\tau = \left(m(\dot{J}\dot{q} + J\ddot{q}) - F\right)J \tag{3.21}$$

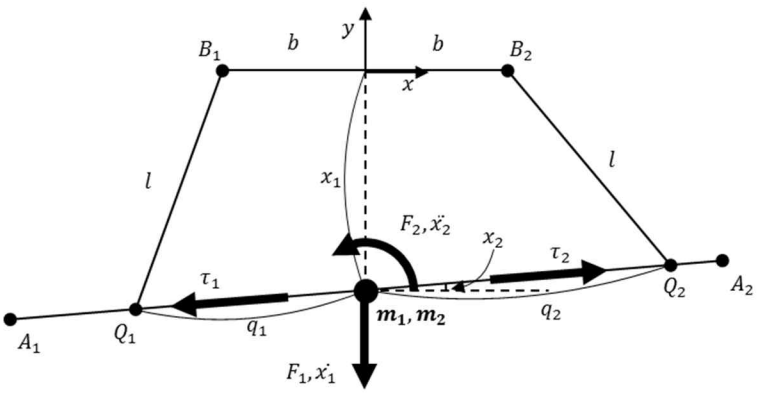

Fig. 3. 3 Dynamic model of the cleaning unit

Chapter 4

Design of force tracking algorithm

4.1 Position-based force tracking impedance control

Impedance controller was introduced by Neville Hogan[17] and provides a control method that enables the interaction between the manipulator and the surrounding environment to follow the characteristics of the designer's desired impedance (mass, spring, damper).

With this controller, compliant movements can be realized in both situations where the wall and the manipulator are in or not in contact. Thus the control algorithm is suitable for use in cleaning units that are difficult to obtain accurate dynamics due to the compliance structure, and also good for the situation where the distance between the wall and the unit continuously changes.

Among the impedance controllers, there are torque-based impedance control and position-based impedance control, and position-based impedance control is also called admittance control. Admittance control has an advantage that it can be applied even if the impedance characteristic of a real manipulator is unknown, but since the manipulator

modeling is not reflected, the convergence is slow and it is difficult to predict the required torque.

In the case of this cleaning unit manipulator, if the platform does not move, the dynamics equation can be expressed as Eq. (3.11). However, additional sensors are needed to quantify the dynamics of the manipulator because the positional acceleration of the joints changes as the robot platform ascends/descends along the wall. In addition, forces are generated through the interaction between the wall and the manipulator and it is impossible to predict the force generated by the compliance structure with nonlinear characteristics.

Therefore, the position-based impedance control can be effectively used in the control of this manipulator and the structure of the applied impedance controller is as follows.

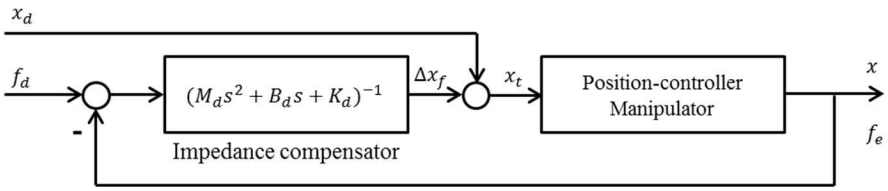

Fig. 4. 1 Block diagram of position-based impedance control

The position-based impedance control is an indirect control method that controls the position-based on the force generated by the interaction between the manipulator and the surrounding environment. The contact force error caused by the interaction between the manipulator and the surrounding environment is measured and the movement trajectory is compensated to have the desired impedance characteristic.

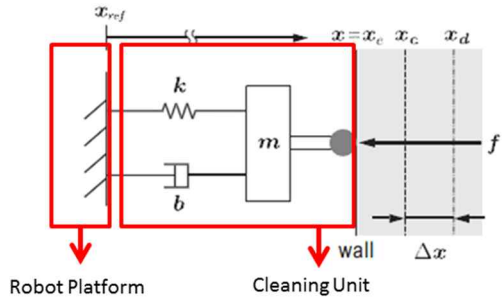

Fig. 4. 2 Equivalent system of the Impedance control

If the position controller is operating ideally (position command and the actual controlled position are the same) the steady-state force tracking error can be expressed as follows.

Target Impedance Equation : $\boldsymbol{M_d\ddot{x}_{dc} + B_d\dot{x}_{dc} + K_dx_{dc} = -E}$ (4.1)

$F = -k_e(x - x_e)$

$K_d(x_{ss} - x_{des}) = -E_{ss} = F_{ss} - F_{ref}$

$K_dx_{ss} - K_dx_{des} = -k_e(x_{ss} - x_e) - F_{ref} \rightarrow x_{ss} = \frac{K_dx_{des} + k_ex_e - F_{ref}}{K_d + k_e}$

$F_{ss} = -k_e\left(\frac{K_dx_{des} + k_ex_e - F_{ref}}{K_d + k_e} - x_e\right) = -\frac{k_e}{K_d + k_e}\left(K_dx_{des} - K_dx_e - F_{ref}\right)$

$$\boldsymbol{E_{ss} = F_{ref} - F_{ss} = \frac{K_dk_e}{K_d + k_e}\left(\frac{F_{ref}}{k_e} + x_{des} - x_e\right)} \quad (4.2)$$

In the above equation, M_d, B_d, K_d are the terms of the target impedance of the manipulator determined by the designer (mass, damper, spring), k_e is the actual stiffness of the environment in which the manipulator touches and x_e is the actual distance between the manipulator and the surrounding environment. As can be seen from the equation, when using the existing impedance compensation formula, the force tracking error is a value dependent of $k_e, K_d, x_e, x_{des}, F_{ref}$. If the above parameters are selected properly, the force

tracking error cab be made to be zero, but the actual environment stiffness k_e is difficult due to the fact that distance between the actual wall and the robot platform continuously changes. Therefore, additional compensation algorithms are required for accurate force tracking.

4.1.1 Position-based force tracking impedance controller design

The impedance model for the proposed position-based impedance control scheme is written as follows:

$$M\ddot{x_{dc}} + B\dot{x_{dc}} + K(t)x_{dc} = -E_f \tag{4.3}$$

where M, B and K are the target mass, damping and stiffness parameters for the impedance control. x_{dc} denotes the trajectory correction defined by the difference between desired and compliant trajectories x_d and x_c of manipulator. Note that the compliant trajectory is used to reflect that the trajectory of environment may change even slightly due to its shape or stiffness. F corresponds to the real contact force.

The proposed position-based impedance control scheme is given by

$$\begin{cases} K(t) = \left(k_p E_f + k_d \dot{E_f} + k_i \int_0^t E_f(\tau) d\tau \right) {x_{dc}}^{-1} + k_0 \\ x_d = x_d^0 + \eta x_{dc} \end{cases} \tag{4.4}$$

where k_0 and x_d^0 denote the modified target stiffness and the initial condition for the desired trajectory, respectively. E_f is the force tracking error defined by the difference between the real contact and reference forces $E_f = F_{ref} - F$, and k_p, k_d and k_i are the proportional, derivative and integral control gains, respectively. η is the positive control gain for the desired trajectory correction.

It is worthwhile to note that the proposed impedance control scheme consists of stiffness adaptation as well as reference position correction, where the target stiffness is adapted by a

PID control using the force tracking error while the reference position is adjusted to improve the force tracking capability effectively. In combination with the stiffness adaptation in Eq. (4.4), Eq. (4.3) becomes

$$M\ddot{x}_{dc} + B\dot{x}_{dc} + k_0 x_{dc} = -(k_p + 1)E_f - k_d\dot{E}_f - k_i\int_0^t E_f(\tau)d\tau \tag{4.5}$$

Since $x_{dc} = x_c - x_d = x_c - x_d^0 - \eta x_{dc}$ and the initial reference position x_d^0 is constant, the first and second derivatives of the trajectory correction are given by

$$\dot{x}_{dc} = \frac{\dot{x}_c}{1+\eta} \text{ and } \ddot{x}_{dc} = \frac{\ddot{x}_c}{1+\eta} \tag{4.6}$$

Substituting Eq. (4.6) into Eq. (4.5) yields

$$M\ddot{x}_c + B\dot{x}_c + k_0 x_c - k_0 x_d^0 = -(\eta+1)\left\{(k_p + 1)E_f + k_d\dot{E}_f + k_i\int_0^t E_f(\tau)d\tau\right\} \tag{4.7}$$

Without loss of generality, it is assumed that the contact force F can be expressed by $F = -k_e(x - x_e)$ where x and x_e are the trajectories of the manipulator and the environment, respectively. k_e is the unknown stiffness of environment. Also, a position tracking error may occur in spite of efforts of the inner-loop position controller for the motor drive, that is, $x_c = x + \delta x$ where δx denotes the position tracking error of inner-loop controller. As a result, the force tracking error is written by

$$E_f = F_{ref} - F = F_{ref} + k_e(x - x_e) \tag{4.8}$$

Eq. (4.8) implies that the real trajectory of the manipulator can be approximated by

$$x = x_e - \frac{F_{ref} - E_f}{k_e} \ (x = x_c) \tag{4.9}$$

It is worthwhile to note that the trajectory x_e and stiffness k_e of environment are

unknown and also, x_e can be changed so that $\ddot{x}_e \neq 0$ and $\dot{x}_e \neq 0$. Under the assumption that the stiffness of environment is constant, the following derivatives can be obtained from Eq. (4.9):

$$\dot{x} = \dot{x}_e - \frac{\dot{F}_{ref} - \dot{E}_f}{k_e} \quad \text{and} \quad \ddot{x} = \ddot{x}_e - \frac{\ddot{F}_{ref} - \ddot{E}_f}{k_e} \tag{4.10}$$

Substituting Eq. (4.10) into Eq. (4.7) gives

$$M\left(\ddot{x}_e - \frac{\ddot{F}_{ref} - \ddot{E}_f}{k_e} + \delta\ddot{x}\right) + B\left(\dot{x}_e - \frac{\dot{F}_{ref} - \dot{E}_f}{k_e} + \delta\dot{x}\right) + k_0\left(x_e - \frac{F_{ref} - E_f}{k_e} + \delta x\right)$$

$$= -(\eta + 1)\left\{(k_p + 1)E_f + k_d\dot{E}_f + k_i\int_0^t E_f(\tau)d\tau\right\} + k_0 x_d^0 \tag{4.11}$$

Supposing that the first and second derivatives of position error of inner-loop controller are relatively smaller than those of the trajectory of environment, let's define a new variable $\overline{x_e}$ by $\overline{x_e} = x_e + \delta x$ which enables to deal with both varying trajectory of environment and undesired position tracking error simultaneously. Using this definition, Eq. (4.11) becomes

$$M\ddot{\overline{x_e}} + B\dot{\overline{x_e}} + k_0\overline{x_e} - \frac{1}{k_e}\left(M\ddot{F}_{ref} + B\dot{F}_{ref} + k_0 F_{ref}\right) = -\frac{1}{k_e}\left(M\ddot{E}_f + B\dot{E}_f + k_0 E_f\right)$$

$$-(\eta + 1)\left\{(k_p + 1)E_f + k_d\dot{E}_f + k_i\int_0^t E_f(\tau)d\tau\right\} + k_0 x_d^0 \tag{4.12}$$

Define the Laplace transforms of the trajectory of environment combined with the position error, the force tracking error, the initial reference trajectory and the reference force as $L\{\overline{x_e}\} = X_e(s)$, $L\{E_f\} = E_f(s)$, $L\{x_d^0\} = X_d^0(s)$ and $L\{F_{ref}\} = F_{ref}(s)$, respectively. Then, in the Laplace domain, Eq. (4.12) can be rewritten by

$$(Ms^2 + Bs + k_0)X_e(s) - \frac{1}{k_e}(Ms^2 + Bs + k_0)F_{ref}(s) = -\frac{1}{k_e}(Ms^2 + Bs + k_0)E_f(s)$$

$$-(\eta + 1)\left\{k_p + 1 + k_d s + \frac{k_i}{s}\right\}E_f(s) + k_0 X_d^0(s) \tag{4.13}$$

After rearranging each term in Eq. (4.13), the following relation between the force tracking error, varying trajectory of environment and the reference force can be obtained as follows:

$$E_f(s) = -\frac{k_e s(Ms^2+Bs+k_0)}{\Lambda(s)} X_e(s) + \frac{s(Ms^2+Bs+k_0)}{\Lambda(s)} F_{ref}(s) + \frac{k_0 k_e s}{\Lambda(s)} X_d^0(s) \qquad (4.14)$$

where $\Lambda(s)$ corresponds to the characteristic equation of transfer function from the trajectory of environment (or the reference force) to the force tracking error given by $\Lambda(s) = Ms^3 + a_0 s^2 + a_1 s + a_2$. M is chosen to be 1 and $a_0 = B + k_e(1+\eta)k_d$, $a_1 = k_0 + k_e(1+k_p)(1+\eta)$ and $a_2 = k_e(1+\eta)k_i$. In fact, $X_d^0(s) = x_d^0/s$ since the initial reference trajectory x_d^0 is assumed to be constant.

The block diagram of proposed position-based impedance control scheme for force tracking of manipulator is described in Fig. 4. 3, where the real contact force is obtained by calibrating the force measured by using the load cell. It is worthwhile to note that in the proposed impedance control scheme, the reference trajectory and the target stiffness are simultaneously updated because these two terms mainly contribute the force tracking error of classic impedance control in the steady state.

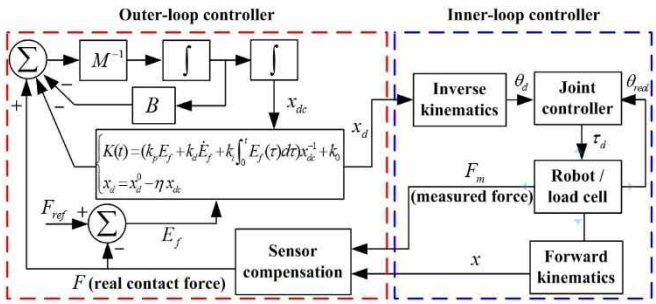

Fig. 4. 3 Block diagram of proposed position-based impedance control scheme for force tracking of manipulator

4.1.2 Stability and performance analysis

In order to derive the stability condition for the proposed position-based impedance control scheme, the Routh-Hurwitz array for Eq. (4.14) is constructed as follows:

s^3	1	a_1
s^2	a_0	a_2
s^1	$(a_0a_1 - a_2)/a_0$	0
s^0	a_2	0

From the Routh-Hurwitz array,
$a_0 > 0,\ a_2 > 0,\ (a_0a_1 - a_2)/a_0 > 0$ should be satisfied to guarantee the stability of proposed impedance control scheme. It should be noted that the proportional, derivative and integral control gains $k_p,\ k_d$ and k_i as well as the trajectory modification gain η are all positive so that $a_i > 0,\ \mathrm{i} = 0, 1$ and 2 are naturally ensured and $a_0a_1 - a_2 > 0$ will guarantee the stability of proposed impedance control law. Recall that the last condition can be rewritten as follows:

$$a_0a_1 - a_2 = \{B + k_ek_d(\eta + 1)\} \times \{k_0 + k_e(k_p + 1)(\eta + 1)\} - k_ek_i(\eta + 1)$$

$$> k_ek_d(\eta + 1) \times k_e(k_p + 1)(\eta + 1) - k_ek_i(\eta + 1)$$

$$> {k_e}^2(\eta + 1)^2((k_p + 1)k_d - \frac{k_i}{k_e(\eta+1)}) > 0$$

From the above inequality, $a_0a_1 - a_2 > 0$ can be guaranteed if

$$(k_p + 1)k_d - \frac{k_i}{k_e(\eta+1)} > 0 \tag{4.15}$$

It is worthwhile to note that k_e can be assumed sufficiently large so that it is easy to choose control gain parameters $k_p,\ k_d,\ k_i$ and η to satisfy Eq. (4.15).

Now, suppose that the trajectory of environment changes as if it is a unit step, that is,

$X_e(s) = 1/s$. For the constant reference force F_{ref} whose Laplace transform is given by $F_{ref}(s) = F_{ref}/s$, the force tracking error E_f in the steady state can be obtained by using the Final Value Theorem as follows:

$$\lim_{t\to\infty} E_f = \lim_{s\to 0} sE_f(s)$$

$$= \lim_{s\to 0} s\left\{\frac{k_e s(Ms^2+Bs+k_0)}{\Lambda(s)}\frac{1}{s} + \frac{s(Ms^2+Bs+k_0)}{\Lambda(s)}F_{ref}(s) - \frac{k_0 k_e s}{\Lambda(s)}X_d^0(s)\right\} = 0 \qquad (4.16)$$

which proves that the proposed impedance control scheme enables the manipulator to track the reference force in the steady state in spite of sudden change in the trajectory of environment. Recall that in fact, the reference force in Eq. (4.16) is equal to a step function, which also implies that the proposed impedance control scheme ensures the zero force tracking error in the steady state even though the reference force changes suddenly.

Compared to existing impedance control methods, the proposed position-based impedance control scheme ensures the zero force tracking performance in the steady state against drastic changes in the trajectory of environment and the reference force without detailed information on the dynamics of robot manipulator. In addition, the control parameters are easily chosen and tuned to satisfy the stability condition for the proposed impedance control scheme.

4.1.3 Force tracking impedance controller gain tuning using root locus

In order to improve the performance of the impedance control, gain tuning was carried out. There are two conditions for the gain tuning. One is rise time which is the smaller-the-better characteristic for contact force adaptation. The other is overshoot which should be kept below 25 % of target force in order to ensure the stability of the mechanical system. Root locus is used as gain tuning method, and the gain tuning sequence is from a relatively unstable poles to a stable poles. The initial gain was $k_i = 5, k_d = 0.01, k_p = 5, \eta = 5$.

If k_i has a value of more than 200, the system becomes unstable as shown in Fig. 4. 4(a). Therefore 20 was chosen to have a safety factor of 10. k_d, k_p and η were selected as $k_d = 0.06, k_p = 6,$ and $\eta = 6,$ respectively, so that the damping coefficient becomes 0.5 in order to have an overshoot of 25 % or less.

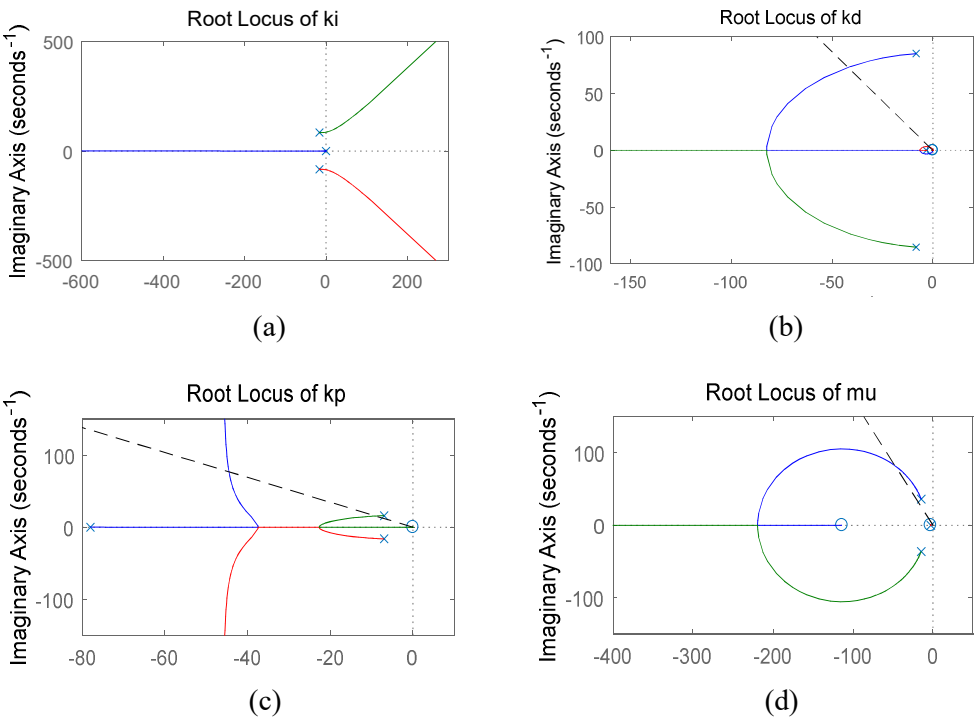

Fig. 4. 4 Root locus of force tracing impedance control about (a) k_i, (b) k_d, (c) k_p, (d) η

In order to evaluate the effect of gain tuning, simulation and experiment were conducted on step and sinusoidal disturbance.

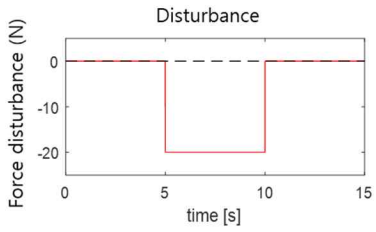

Fig. 4. 5 Disturbance of 20 N, step

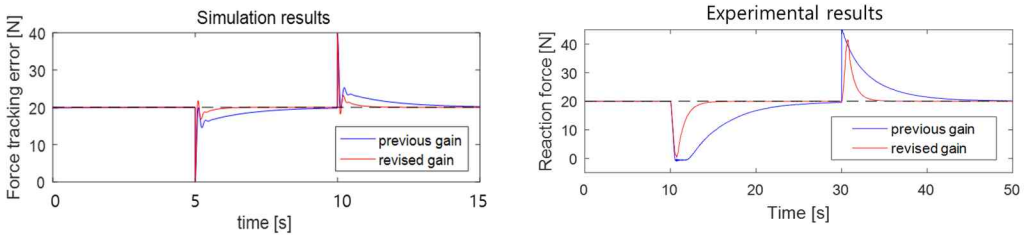

(a) (b)

Fig. 4. 6 (a) Simulation and (b) experimental results of step disturbance with variable gains

In the simulation, the settling time is reduced by 77 % from 1.3 s to 0.3 s when the revised gain was used. And the experiment show that the settling time was reduced by 84 % from 20.0 s to 3.3 s.

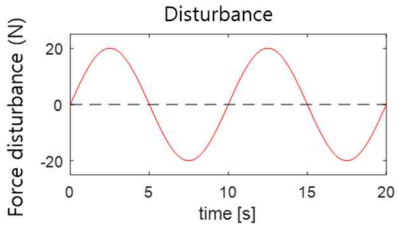

Fig. 4. 7 Disturbance of 0.1 Hz sinusoidal, 20 N

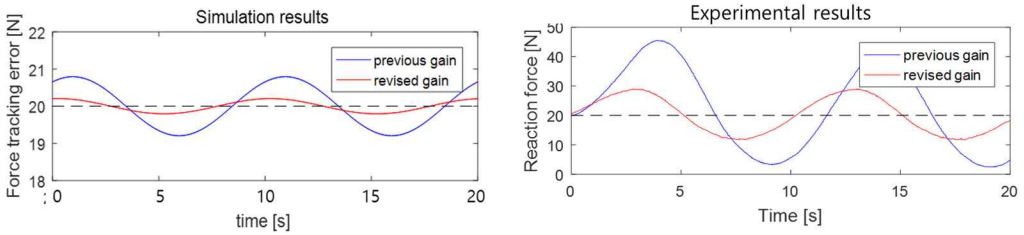

(a) (b)

Fig. 4. 8 (a) Simulation and (b) experimental results of sinusoidal disturbance with variable gains

In the simulation, the maximum difference is reduced by 75 % from 1.6 N to 0.4 N when the revised gain was used. And the experiment show that the maximum difference was reduced by 55 % from 38.5 N to 17.3 N.

4.2 Disturbance compensation algorithm

Impedance-based control, as demonstrated in the previous chapter, allows the target force tracking for distances that change stepwise. But since the dynamics of the manipulator is not reflected in the controller, the force tracking speed is slow for an instantaneous change of disturbance or a continuously changing disturbance. In actual working environment, it is necessary to cope with disturbance effectively because there are obstacles such as window frame on the outer wall and the distance between the wall and unit during the climbing process of the robot platform. To solve the foresaid problem, a disturbance compensation algorithm was added. A controller is developed to compensate the disadvantages of the two controls by using a disturbance observer and a sliding mode controller. The stability of the controller is verified through experiments. The overall control strategy is shown in the following block diagram.

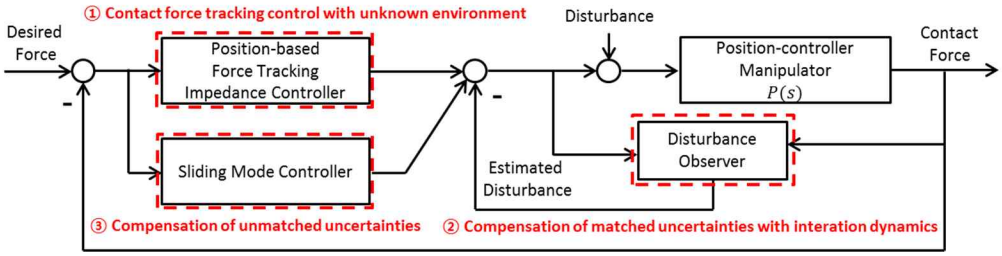

Fig. 4. 9 Control strategy of cleaning unit

4.2.1 Disturbance observer design

When designing a controller and applying it to a real plant, disturbance often has a negative effect on control performance. Therefore, it is one of the important problems to compensate the disturbance to improve the control performance in the actual control system. Disturbance can be divided into two: disturbance acting from the outside of the system, disturbance inside the system. Disturbances acting inside the system include unmodeled dynamics and errors in dynamic model parameters. It is very difficult for conventional controllers (PID, LQR, etc.) to cope with severe disturbances and uncertainty unless

additional controllers are designed for disturbances. [18,19]

Various controllers such as adaptive controller, robust controller, sliding mode controller and feedforward controller have been developed to compensate disturbance.

The adaptive controller is a method of estimating the time varying model parameters and is widely used. However, it is difficult to calculate the nonlinear dynamics model and it is difficult to accurately update the parameter value when the disturbance is large during the experiment.

Sliding mode controllers can effectively respond to parameter uncertainties, but the switching mechanism often causes chattering problems when applied to real mechanical systems.

Feedforward controller actively removes disturbance by measuring disturbance and system response due to disturbance. But it is difficult to accurately extract disturbance in actual mechanical system, and it is disadvantageous to use expensive measuring instrument for accurate measurement.

To overcome the disadvantages of the above controllers, disturbance observer is used. It is often used in a practical industrial field because it has strong disturbance reduction compared to its simple structure.

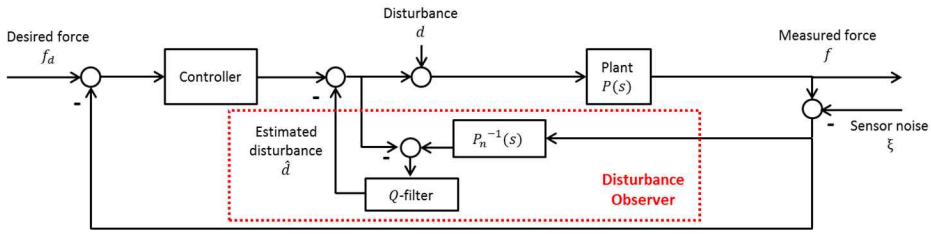

Fig. 4. 10 Block diagram of disturbance observer

The above block diagram is the structure of the basic disturbance observer. When the plant model to be controlled is $P(s)$, and the nominal model is $P_n(s)$, term $W_2(s)$ corresponding to the parameter uncertainty of the plant can be defined as follows.

$$P(s) = P_n\big(1 + W_2(s)\Delta(s)\big) \text{ with } \|\Delta(s)\|_\infty \le 1 \tag{4.17}$$

$W_2(s)\Delta(s)$ corresponds to the error of the plant model and Lumped disturbance d_l can be defined including the error of the plant model and the external disturbance d[20].

$$\{U_t(s) + D\}P_n\big(1 + W_2(s)\Delta(s)\big) = \{U_t(s) + D_l\}P_n \tag{4.18}$$

$$D_l(s) = \big(1 + W_2(s)\Delta(s)\big)D(s) + W_2(s)\Delta(s)U_t(s) \tag{4.19}$$

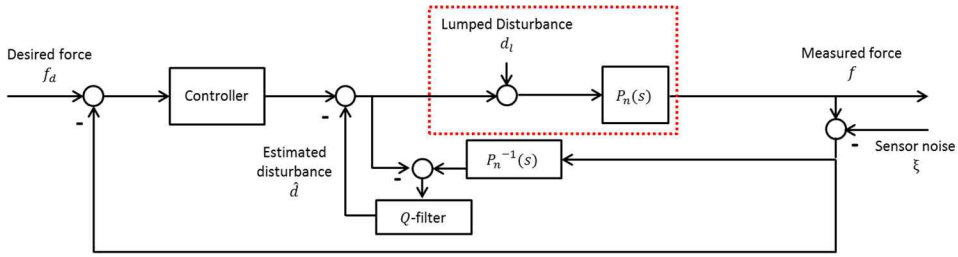

Fig. 4. 11 Block diagram of disturbance observer

The Laplace transform of each term is expressed as

$\mathcal{L}\{d\} = D(s)$, $\mathcal{L}\{\hat{d}\} = \hat{D}(s)$, $\mathcal{L}\{d_l\} = D_l(s)$, $\mathcal{L}\{\xi\} = \Xi(s)$

Lumped disturbance can be expressed as

$$D_l(s) = P(s){P_n}^{-1}(s)D(s) + \big\{P(s){P_n}^{-1}(s) - 1\big\}U_t(s) \tag{4.20}$$

$$\begin{aligned}\hat{D}(s) &= Q(s)\left[-U_t(s) + {P_n}^{-1}(s)\{F(s) - \Xi(s)\}\right] \\ &= Q(s)\left[-U_t(s) + {P_n}^{-1}(s)P_n(s)\{U_t(s) + D_l(s)\} - {P_n}^{-1}(s)\Xi(s)\right] \\ &= Q(s)D_l(s) - Q(s){P_n}^{-1}(s)\Xi(s)\end{aligned} \tag{4.21}$$

Therefore, the error dynamics of the lumped disturbance estimation is as follows.

$E_d(s) = \hat{D}(s) - D_l(s) = \{Q(s) - 1\}D_l(s) - Q(s){P_n}^{-1}(s)\Xi(s)$

$$=\{Q(s)-1\}\left[P(s){P_n}^{-1}(s)D(s)+\left\{P(s){P_n}^{-1}(s)-1\right\}U_t(s)\right]-Q(s){P_n}^{-1}(s)\Xi(s) \quad (4.22)$$

Due to the nature of the mechanical system, disturbance is dominant at low frequency and sensor noise is dominant at high frequency. Therefore, in order to neglect the effect of sensor noise and to maximize the disturbance attenuation effect, it is general to design a Q-filter with low-pass filter characteristic with $\lim_{w\to 0} Q(jw)=1$, $\lim_{w\to\infty} Q(jw)=0$. The error dynamics at this point is as follows.

$$\lim_{w\to 0} E_d(jw)=-{P_n}^{-1}(jw)\Xi(jw)\approx 0$$

$$\lim_{w\to\infty} E_d(jw)=-\left[P(jw){P_n}^{-1}(jw)D(jw)+\left\{P(jw){P_n}^{-1}(jw)-1\right\}U_t(jw)\right]$$

$$\approx -\left\{P(jw){P_n}^{-1}(jw)-1\right\}U_t(jw)$$

Especially when $P(s)=P_n(s)$, the error dynamics converges to 0 regardless of the frequency of disturbance. It is very important in disturbance observer to select appropriate dimension of Q-filter and cut-off frequency to observe disturbance in the workspace and to minimize the influence of noise.

4.2.1.1 System identification of cleaning unit

The cleaning unit generates force through the interaction between the wall and the manipulator. However, due to the compliance structure with nonlinear characteristics, it is impossible to obtain the reaction force quantitatively through the dynamics equation. Therefore, the position-based impedance controller is used and the dynamics equation of the cleaning unit itself is not used since it is not torque-based control. Instead of analyzing dynamics of the cleaning unit, the interaction between the cleaning unit and the surrounding environment is modeled. The disturbance observer is suitable as the controller of the main cleaning unit because it can be used when the uncertainty of the system model parameter exists around the nominal plant.

The modeling of the interaction between the cleaning unit and the surrounding environment was performed using a frequency response experiment for disturbances of 8 mm amplitude at 0.1 Hz to 1.5 Hz.

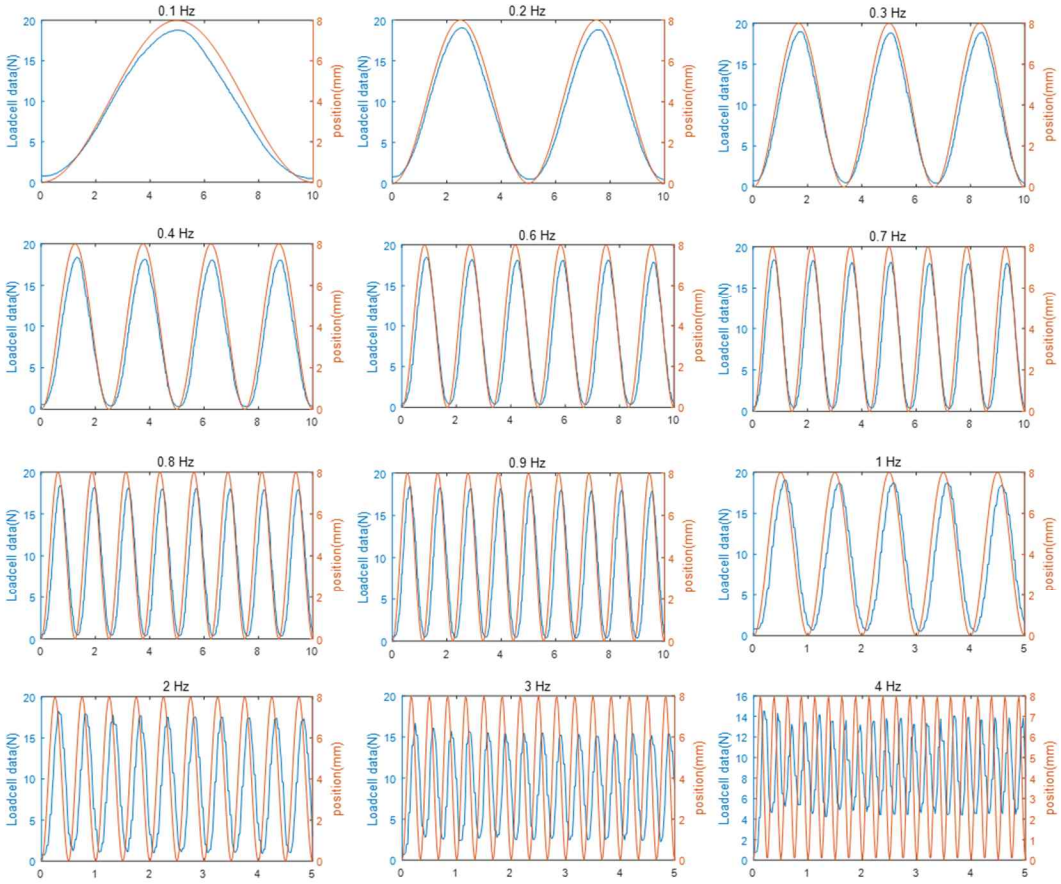

Fig. 4. 12 Frequency response experiment data

For frequency response experiments, Bode plot for magnitude and phase as follows.

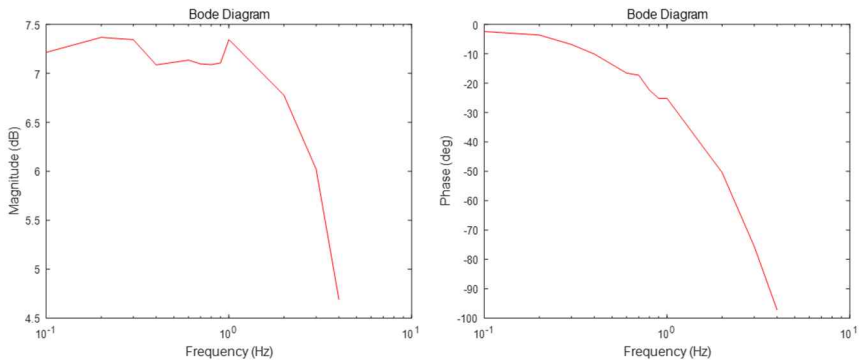

Fig. 4. 13 Bode plot from frequency response experiment data

Assuming that the displacement model of the cleaning unit and the external environment is a transfer function with two poles and one zero, the median and upper and lower limits of each parameter can be obtained by the bode plot as follows.

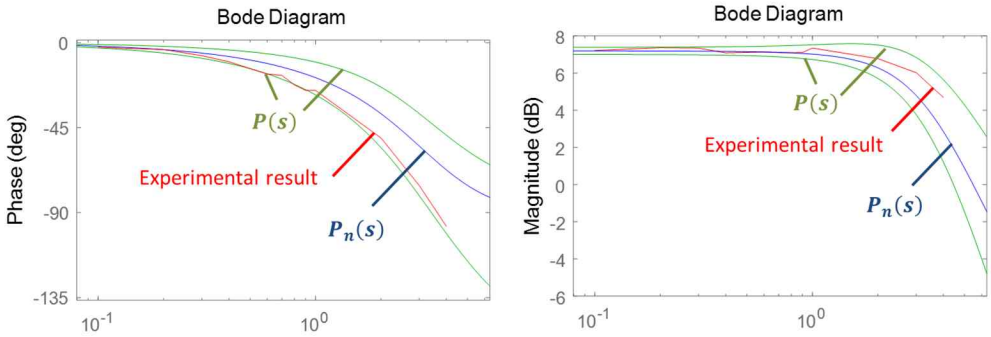

Fig. 4. 14 Bode plot of plant model and experimental data

Nominal plant model of cleaning unit : $P_n(s) = \frac{28s+1030}{s^2+35s+450}$ (4.23)

$a_0 = a_{1,n} \pm 2\ \%$, $a_1 = 35$, $b_0 = 1030$, $b_1 = b_{1,n} \pm 100\ \%$

Where $a_{0,n} = 450$, $b_{1,n} = 28$

4.2.1.2 Q-filter design of disturbance observer

It is important to design a Q-filter with a proper cut-off frequency in order to observe and compensate for disturbances and to prevent the system from becoming unstable due to sensor noise.

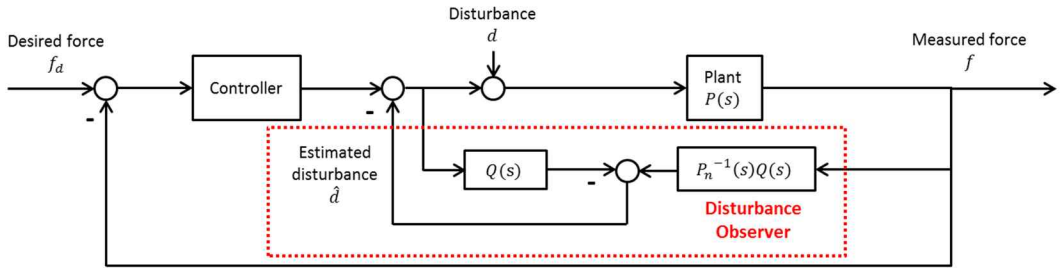

Fig. 4. 15 Block diagram of disturbance observer

For the input of the system to be stable, $Q(s)$ and $P_n{}^{-1}(s)Q(s)$ must be proper transfer functions, therefore, relative degree ρ_P of P_n should be smaller than relative degree ρ_Q of Q, and the order N of $Q(s)$ must satisfy the following equation.

$$\mathrm{N} \geq \rho_P + n - 1 \tag{4.24}$$

The relative degree ρ_P of P_n obtained from the system identification of the cleaning unit is 1, and the sinusoidal disturbance should have $\mathrm{N} \geq 2$ since the order of the denominator of the transfer function form is 2. In this case, the larger the ρ_Q, the greater the noise rejection effect and the less the peaking of the frequency response, so ρ_Q = 3 was selected in this controller.

Therefore, the transfer function form of Q-filter is as follows.

$$\mathrm{Q(s)} = \frac{1 + \mathrm{a}_1(\tau \mathrm{s})}{1 + \mathrm{a}_1(\tau \mathrm{s}) + \mathrm{a}_2(\tau \mathrm{s})^2 + \mathrm{a}_3(\tau \mathrm{s})^3 + \mathrm{a}_4(\tau \mathrm{s})^4} \tag{4.25}$$

a_1, a_2, a_3 are coefficients of Butterworth or binomial polynomials. Controller design of the cleaning unit used coefficients of Butterworth.

4.2.1.3 Stability analysis of disturbance observer

In order to show the stability of the disturbance observer, it is necessary to primarily define the uncertainty. The relation between plant in real system and nominal plant can be expressed as follows using uncertainty term.

$$P(s) = (1 + W_2(s)\Delta(s))P_n(s) \qquad \text{with} \quad \|\Delta(s)\|_\infty \leq 1$$

To satisfy $\|\Delta(s)\|_\infty \leq 1$, the following equation must be established.

$$\max\left|\frac{P(jw)-P_n(jw)}{P_n(jw)}\right| \leq |W_2(jw)| \qquad \forall w \in R \tag{4.26}$$

Therefore, the transfer function of the uncertainty term, which is greater than or equal to the maximum value of $\left|\frac{P(jw)-P_n(jw)}{P_n(jw)}\right|$ in the range of the parameter of the plant, is obtained through the bode plot.

$$W_2 = \frac{1+\frac{s}{0.004}}{1+\frac{s}{0.0001}} \cdot \frac{1+\frac{s}{0.6}}{1+\frac{s}{25}} \tag{4.27}$$

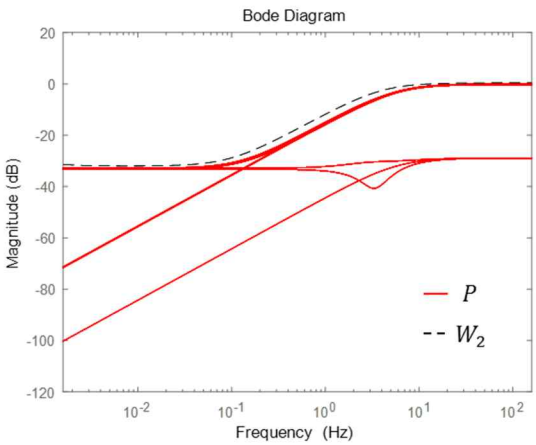

Fig. 4. 16 Bode plot from uncertainty transfer function

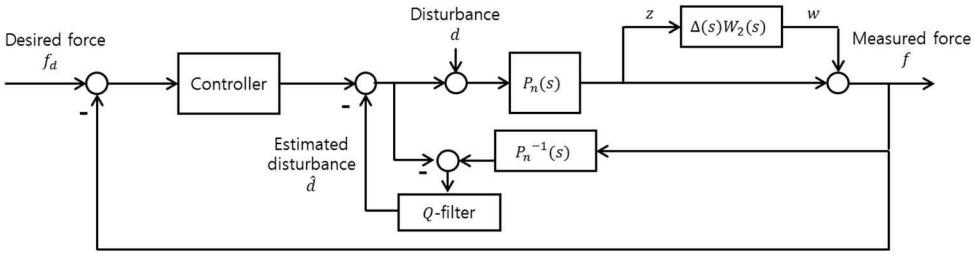

Fig. 4. 17 Block diagram of disturbance observer

The relationship between z and w in the above block diagram is as follows.

$$w = \Delta(s)W_2(s)z \tag{4.28}$$

$$f = z + w = \big(1 + \Delta(s)W_2(s)\big)z = \frac{1+\Delta(s)W_2(s)}{\Delta(s)W_2(s)}w \tag{4.29}$$

$$z = P_n(s)u_1 \tag{4.30}$$

$$\big(1 - Q(s)\big)u_1 = -Q(s){P_n}^{-1}(s)f \tag{4.31}$$

Substituting Eq. (4.29) and (4.30) into Eq. (4.31) gives

$$\big(1 - Q(s)\big){P_n}^{-1}(s)z = -Q(s){P_n}^{-1}(s)f \tag{4.32}$$

$$\frac{f}{z} = \frac{Q(s)-1}{Q(s)} = \big(1 + \Delta(s)W_2(s)\big) \tag{4.33}$$

$$\frac{w}{z} = \Delta(s)W_2(s) = -\frac{1}{Q} \tag{4.34}$$

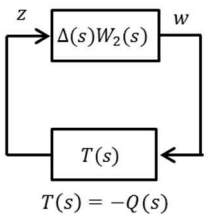

By small gain theorem

The DOB feedback loop is robustly stable if and only if :

$$\|W_2(s)Q(s)\|_\infty < 1 \ , \ \therefore \quad \|Q(s)\|_\infty < \left\|W_2{}^{-1}(s)\right\|_\infty \tag{4.35}$$

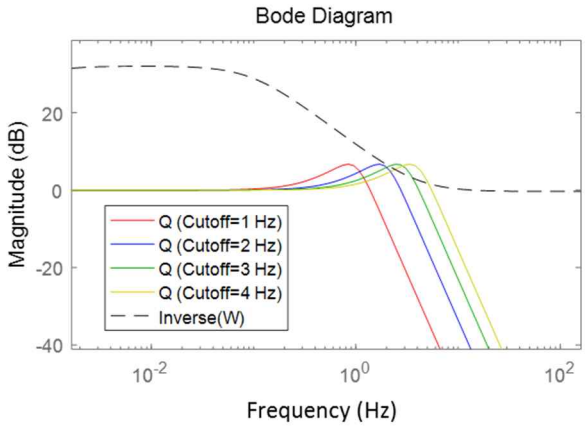

Fig. 4. 18 Bode plot for Q-filter design

The above bode plot shows that the controller is stable for a cut-off frequency of 1 to 2 Hz. On the other hand, at the cut-off frequency of 3 Hz or more, the frequency is greater than uncertainty depending on the frequency of the disturbance, which is unstable.

4.2.1.4 Stability analysis of whole control system

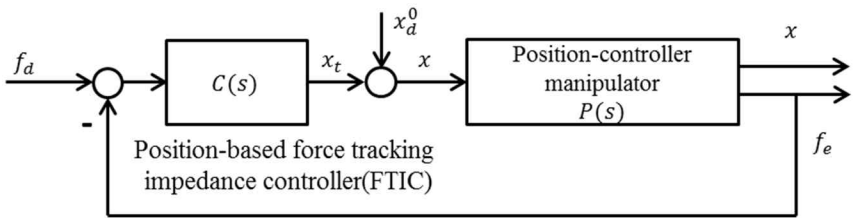

Fig. 4. 19 Block diagram of position-based force tracking impedance controller

The position-based force tracking impedance controller is shown in the form of transfer function as follows.

Target impedance model : $M\ddot{x_{dc}} + B\dot{x_{dc}} + K(t)x_{dc} = -E_f$

Adaptation law : $\begin{cases} K(t) = \left(k_p E_f + k_d \dot{E_f} + k_i \int_0^t E_f(\tau)d\tau\right) {x_{dc}}^{-1} + k_0 \\ x_d = x_d^0 + \eta x_{dc} \end{cases}$

$M\ddot{x_{dc}} + B\dot{x_{dc}} + k_0 x_{dc} = -(1 + k_p)E_f - k_d \dot{E_f} - k_i \int_0^t E_f(\tau)d\tau$

The Laplace transform of above equation is

$$Ms^2 X_{dc} + BsX_{dc} + k_0 X_{dc} = -(1 + k_p)E_f - k_d s E_f - \frac{k_i E_f}{s} \tag{4.36}$$

$$\therefore \ \frac{X_{dc}(s)}{E_f(s)} = \frac{-k_d s^2 - (1+k_p)s - k_i}{Ms^3 + Bs^2 + k_0 s} \tag{4.37}$$

$$\frac{X_t(s)}{X_{dc}(s)} = \eta + 1 \quad (x_t = x - x_d^0) \tag{4.38}$$

$$\therefore \ C(s) = \frac{X_{dc}(s)}{E_f(s)} \frac{X_t(s)}{X_{dc}(s)} = -(\eta + 1) \frac{k_d s^2 + (k_p+1)s + k_i}{Ms^3 + Bs^2 + k_0 s} \tag{4.39}$$

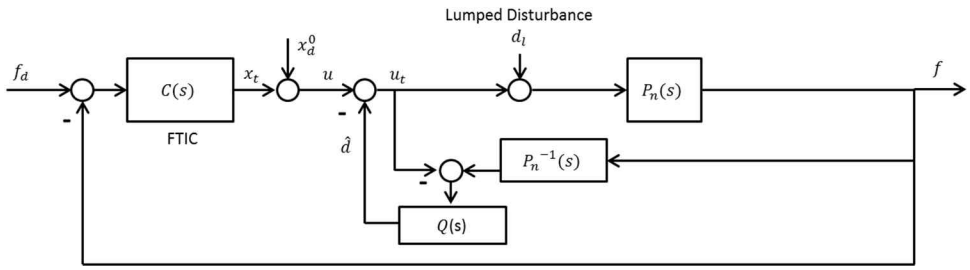

Fig. 4. 20 Block diagram with the disturbance observer added to the position-based force tracking impedance controller

The block diagram with the disturbance observer added to the position-based force tracking impedance controller is shown in the Fig. 4.15.

The relationship between z and w in the above block diagram is as follows.

$$w = \Delta(s)W_2(s)z \tag{4.40}$$

$$f = z + w = \big(1 + \Delta(s)W_2(s)\big)z = \frac{1+\Delta(s)W_2(s)}{\Delta(s)W_2(s)}w \tag{4.41}$$

$$z = P_n(s)u_t \tag{4.42}$$

$$\frac{f}{z} = \frac{Q-1}{P_n(s)C(s)+Q(s)} = 1 + \Delta(s)W_2(s) \tag{4.43}$$

$$\therefore \quad \frac{w}{z} = \frac{-P_n(s)C(s)-1}{P_n(s)C(s)+Q(s)} \tag{4.44}$$

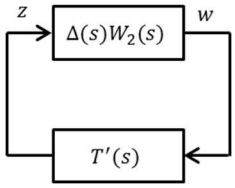

$$T'(s) = -\frac{P_n(s)C(s) + Q(s)}{P_n(s)C(s) + 1} \tag{4.45}$$

By small gain theorem, the overall control system is robustly stable if and only if :

$$\|W_2(s)T'(s)\|_\infty < 1 \quad \therefore \quad \|T'(s)\|_\infty < \left\|{W_2}^{-1}(s)\right\|_\infty \tag{4.46}$$

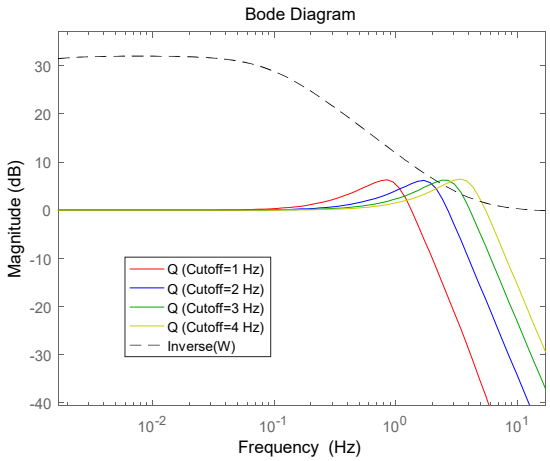

Fig. 4. 21 Bode plot of overall control system

The above bode plot shows that the overall control system is stable for a cut-off frequency of 1 to 2 Hz. On the other hand, at the cut-off frequency of 3 Hz or more, the frequency is greater than uncertainty depending on the frequency of the disturbance, which is unstable.

4.2.1.5 Performance analysis

In the above block diagram, the following equation for error dynamics of estimated disturbance can be obtained. The estimated disturbance is as follows

$$P(s) = (1 + W_2(s)\Delta(s))P_n(s) \qquad \text{with} \quad \|\Delta(s)\|_\infty \leq 1 \tag{4.47}$$

$$\mathcal{L}\{d\} = D(s)\,,\ \mathcal{L}\{\hat{d}\} = \hat{D}(s)\,, \mathcal{L}\{d_l\} = D_l(s) \tag{4.48}$$

$$\begin{aligned} D_l(s) &= P(s){P_n}^{-1}(s)D(s) + \{P(s){P_n}^{-1}(s) - 1\}U_t(s) \\ &= \big(1 + W_2(s)\Delta(s)\big)D(s) + W_2(s)\Delta(s)U_t(s) \end{aligned} \tag{4.49}$$

$$\widehat{D}(s) = Q(s)\{-U_t(s) + {P_n}^{-1}(s)F(s)\}$$

$$\therefore \quad \widehat{D}(s) = Q(s)\left[-U_t(s) + {P_n}^{-1}(s)P_n(s)\{U_t(s) + D_l(s)\}\right] = Q(s)D_l(s) \tag{4.50}$$

Therefore, the error dynamics of the estimated disturbance is as follows.

$$\frac{E_d(s)}{D_l(s)} = \frac{\widehat{D}(s) - D_l(s)}{D_l(s)} = Q(s) - 1 \tag{4.51}$$

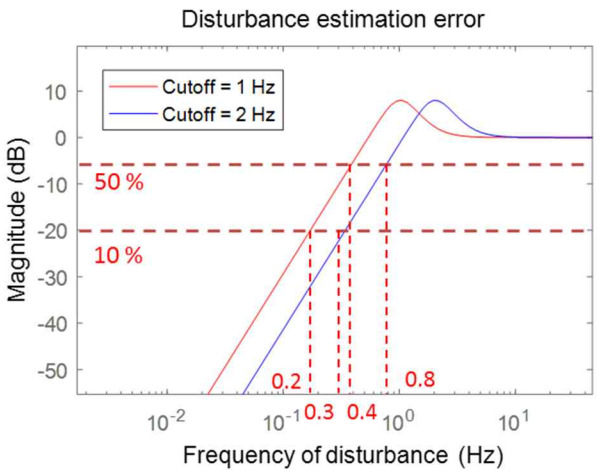

Fig. 4. 22 Disturbance estimation error of Q-filter

The error dynamics of the overall control system can be obtained.

From the block diagram

$$U_t(s) = U(s) - \widehat{D}(s) \tag{4.52}$$

$$U(s) = C(s)\{F_d(s) - F(s)\} + {X_d}^0(s) \tag{4.53}$$

$$U_t(s) = C(s)F_d(s) - C(s)F(s) + {X_d}^0(s) - Q(s)D_l(s)$$

$$= C(s)F_d(s) - C(s)P_n(s)\{U_t(s) + D_l(s)\} + {X_d}^0(s) - Q(s)D_l(s)$$

$$\{1 + C(s)P_n(s)\}\boldsymbol{U_t(s)} = C(s)F_d(s) - C(s)P_n(s)D_l(s) + {X_d}^0(s) - Q(s)D_l(s)$$

$$= C(s)F_d(s) + {X_d}^0(s) - \{C(s)P_n(s) + Q(s)\}D_l(s)$$

$$= C(s)F_d(s) + {X_d}^0(s) - \{C(s)P_n(s) + Q(s)\}[P(s){P_n}^{-1}(s)D(s)$$

$$+\{P(s){P_n}^{-1}(s) - 1\}U_t(s)]$$

Total control input U_t is obtained as follows :

$$U_t(s) = \frac{C(s)F_d(s)+{X_d}^0(s)-C(s)P(s)D(s)-Q(s)P(s){P_n}^{-1}(s)D(s)}{1+C(s)P(s)+Q(s)P(s){P_n}^{-1}(s)-Q(s)}$$

$$= \frac{C(s)F_d(s)+{X_d}^0(s)-\{C(s)P_n(s)+Q(s)\}\big(1+W_2(s)\Delta(s)\big)D(s)}{1+C(s)P_n(s)+\{C(s)P_n(s)+Q(s)\}W_2(s)\Delta(s)} \quad (4.54)$$

$$\widehat{D}(s) = Q(s)D_l(s) = Q(s)\big\{\big(1 + W_2(s)\Delta(s)\big)D(s) + W_2(s)\Delta(s)U_t(s)\big\} \quad (4.55)$$

Therefore, the error dynamics of the whole control system can be obtained as follows.

$$E(s) = C^{-1}(s)\big\{U(s) - {X_d}^0(s)\big\} = C^{-1}(s)\big\{U_t(s) + \widehat{D}(s) - {X_d}^0(s)\big\} \quad (4.56)$$

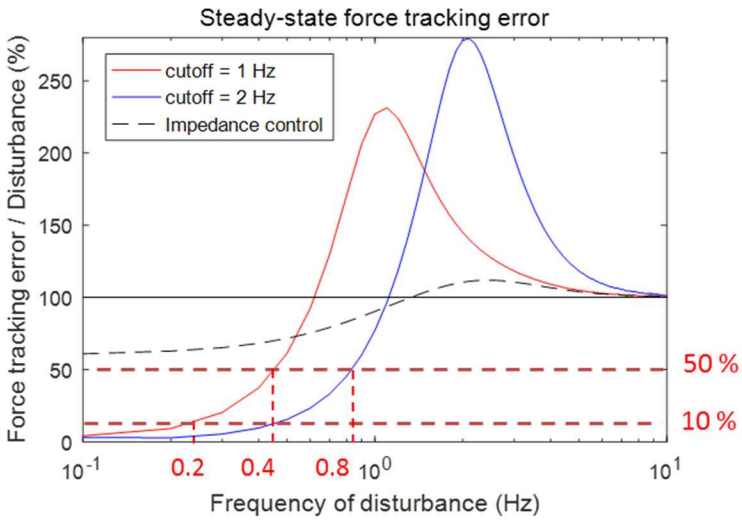

Fig. 4. 23 Error dynamics of the whole control system

4.2.2 Sliding mode controller design

Sliding mode control is one of the widely used control algorithms to compensate for disturbances and plant parameters. While its control structure is quite simple, but it has excellent performance and is used in many industrial plants. Due to the sliding surface structure, it is more sensitive to mismatched uncertainties than matched uncertainties. [21]

In the control of the cleaning unit, the disturbance observer estimates the disturbance based on the interaction modeling between the cleaning unit and the external environment. Due to the nature of the Q-filter, both disturbance estimation and rejection performance are inevitably low for disturbances with frequency bands near the cut-off frequency. Therefore, disturbances which cannot be estimated by disturbance observer can be regarded as mismatched disturbances. Disturbances that cannot be compensated by the disturbance observer can be compensated using the sliding mode control.

4.2.2.1 Sliding mode surface design

From the impedance control problem

$$\mathrm{M}\ddot{x}_{dc} + B\dot{x}_{dc} + k_0 x_{dc} = -E_f - k_p E_f - k_d \dot{E}_f - k_i \int_0^t E_f(\tau)d\tau \tag{4.57}$$

To discretize the above impedance equation,[22]

$\dot{x}_{dc},\ \ddot{x}_{dc},\ \dot{E}_f,\ \int_0^t E_f(\tau)d\tau$ can be expressed by the discretized form

$$\dot{x}_{dc} \approx \frac{1}{T}(x_{dc,k} - x_{dc,k-1}),\ \ddot{x}_{dc} \approx \frac{1}{T^2}(x_{dc,k} - 2x_{dc,k-1} + x_{dc,k-2})$$
$$\dot{E}_f \approx \frac{1}{T}(E_{f,k} - E_{f,k-1}) \tag{4.58}$$

$$\int_0^t E_f(\tau)d\tau \approx T\left(E_{f,k} + E_{f,k-1} + \cdots + E_{f,1}\right) = TE_{f,k} + TE_{f,k-1} + TS_{k-2} \tag{4.59}$$

Where $S_k = E_{f,k} + E_{f,k-1} + \cdots + E_{f,1}$

Therefore, the discretized impedance equation is as follows.

$$\bar{M}x_{dc,k-2} + \bar{B}x_{dc,k-1} + \bar{K}x_{dc,k} = -E_{f,k} - \overline{b_1}E_{f,k-1} - \overline{b_2}E_{f,k} - \overline{b_3}S_{k-2} \quad (4.60)$$

Where $\bar{M} = \frac{M}{T^2}$, $\bar{B} = \frac{-2M}{T^2} - \frac{B}{T}$, $\bar{K} = \frac{M}{T^2} + \frac{B}{T} + k_0$

$$\bar{b}_1 = -\frac{K_d}{T} + k_i T,\ \bar{b}_2 = k_p + \frac{K_d}{T} + k_i T,\ \bar{b}_3 = k_i T$$

Therefore sliding function is defined as follows

$s = \acute{E}_f + K_2 s_{k-1}$

$s_k = cE_{f,k} + K_2 s_{k-1}$

$$= -c\left(\bar{M}x_{dc,k-2} + \bar{B}x_{dc,k-1} + \bar{K}x_{dc,k} + \overline{b_1}E_{f,k-1} + \overline{b_2}E_{f,k} + \overline{b_3}S_{k-2}\right) + K_2 s_{k-1}$$

Equivalent control input is solution to $\Delta s_k = s_k - s_{k-1} = 0$

$$-c\left(\bar{M}x_{dc,k-2} + \bar{B}x_{dc,k-1} + \bar{K}x_{dc,k} + \overline{b_1}E_{f,k-1} + \overline{b_2}E_{f,k} + \overline{b_3}S_{k-2}\right) + K_2 s_{k-1}$$

$$= s_{k-1} \quad (4.61)$$

$$\bar{K}x_{dc,k} = -\bar{M}x_{dc,k-2} - \bar{B}x_{dc,k-1} - \bar{b}_1 E_{f,k-1} - \bar{b}_2 E_{f,k} - \overline{b_3}S_{k-2} + \frac{K_2 - 1}{c}s_{k-1} \quad (4.62)$$

$u_k^{eq} = x = x_{d,k} + x_{dc,k} = x_d{}^0 + (\eta + 1)x_{dc},$

$$= x_d{}^0 + \frac{\eta+1}{\bar{K}}[-\bar{M}x_{dc,k-2} - \bar{B}x_{dc,k-1} - \bar{b}_1 E_{f,k-1} - \bar{b}_2 E_{f,k} - \overline{b_3}S_{k-2} + \frac{K_2 - 1}{c}s_{k-1}]$$

Switching control input is $u_k^{sw} = K_s \,\mathrm{sign}(s_{k-1})$ and disturbance observer input is

$$u_k^{DOB} = -\hat{d}$$

Total control input is as follows :

$$u_k = u_k^{eq} + u_k^{sw} + u_k^{DOB} \quad (4.63)$$

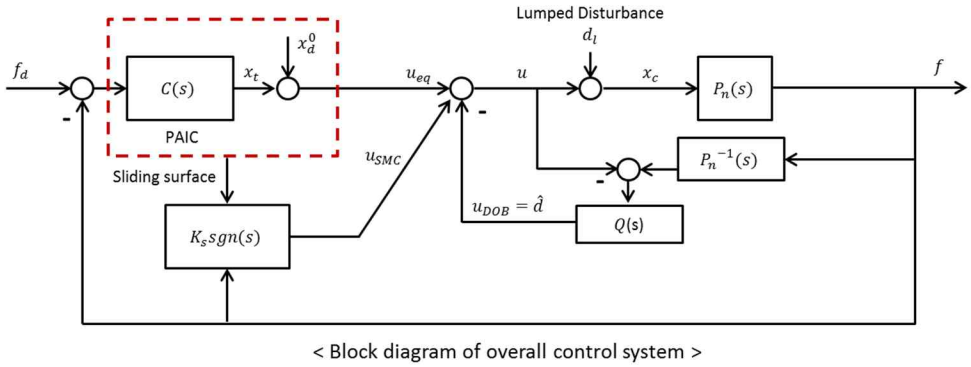

Fig. 4. 24 Block diagram of overall control system

4.2.2.2 Stability analysis

In order for the discretized sliding mode controller to be stable, the system must gradually converge to the sliding surface when the control input is applied to the system. Therefore, applying total control input to s_k, the equation is as follows.

$$s_k = -c\left(\bar{M}x_{dc,k-2} + \bar{B}x_{dc,k-1} + \bar{K}x_{dc,k} + \overline{b_1}E_{f,k-1} + \overline{b_2}E_{f,k} + \overline{b_3}S_{k-2}\right) + K_2 s_{k-1}$$

$$= -c\left(\bar{M}x_{dc,k-2} + \bar{B}x_{dc,k-1} + \bar{K}(x_{c,k} - x_{d,k}) + \overline{b_1}E_{f,k-1} + \overline{b_2}E_{f,k} + \overline{b_3}S_{k-2}\right) + K_2 s_{k-1}$$

$x_{c,k}$: Compliant trajectory (actual postion), d_l : actual disturbance added to the system

$\tilde{d} = d_l - \hat{d}_l$: estimation error of disturbance observer, Ks : sliding mode control gain

$$s_k = -c(\bar{M}x_{dc,k-2} + \bar{B}x_{dc,k-1} + \bar{K}\left(u + d_l - x_{d,k}\right) + \overline{b_1}E_{f,k-1} + \overline{b_2}E_{f,k} +$$

$$\overline{b_3}S_{k-2}) + K_2 s_{k-1}$$

$$= -c(\bar{M}x_{dc,k-2} + \bar{B}x_{dc,k-1} + \bar{K}\left(u_k^{eq} + u_k^{sw} + u_k^{DOB} + d_l - x_{d,k}\right) + \overline{b_1}E_{f,k-1} + \overline{b_2}E_{f,k}$$

$$+\overline{b_3}S_{k-2}) + K_2 s_{k-1}$$

$$= -c(\bar{M}x_{dc,k-2} + \bar{B}x_{dc,k-1} + \bar{K}(x_{c,k} + K_s\,\mathrm{sign}(s_{k-1}) - \hat{d}_l + d_l - x_{d,k})$$

$$+\overline{b_1}E_{f,k-1} + \overline{b_2}E_{f,k} + \overline{b_3}S_{k-2}) + K_2 s_{k-1}$$

$$= -c\bar{M}x_{dc,k-2} + \bar{B}x_{dc,k-1} + \bar{K}\left(x_{dc,k} + K_s \operatorname{sign}(s_{k-1}) + \tilde{d}\right) + \overline{b_1}E_{f,k-1} + \overline{b_2}E_{f,k}$$

$$+\overline{b_3}S_{k-2} + K_2 s_{k-1}$$

$$= -c\left(\bar{M}x_{dc,k-2} + \bar{B}x_{dc,k-1} - \bar{M}x_{dc,k-2} - \bar{B}x_{dc,k-1} - \bar{b}_1 E_{f,k-1} - \bar{b}_2 E_{f,k} - \overline{b_3}S_{k-2} + \right.$$

$$\left.\frac{K_2-1}{c}s_{k-1} + \bar{K}(K_s \operatorname{sign}(s_{k-1}) + \tilde{d}) + \overline{b_1}E_{f,k-1} + \overline{b_2}E_{f,k} + \overline{b_3}S_{k-2}\right) + K_2 s_{k-1}$$

$$= -c\left(\frac{K_2-1}{c}s_{k-1} + \bar{K}(K_s \operatorname{sign}(s_{k-1}) + \tilde{d})\right) + K_2 s_{k-1}$$

$$= -c\left(\frac{K_2-1}{c}s_{k-1} + \bar{K}(K_s \operatorname{sign}(s_{k-1}) + \tilde{d})\right) + K_2 s_{k-1}$$

$$= s_{k-1} - c\bar{K}(K_s \operatorname{sign}(s_{k-1}) + \tilde{d})$$

If $s_{k-1} > 0$ and $K_s \geq |\tilde{d}|$ are satisfied, then $s_k \leq s_{k-1}$

If $s_{k-1} < 0$ and $K_s \geq |\tilde{d}|$ are satisfied, then $s_k \geq s_{k-1}$

Therefore, the sliding mode controller is stable when the following condition is satisfied.

$$|s_k| \leq |s_{k-1}| \text{ if } K_s \geq |\tilde{d}| \tag{4.64}$$

Chapter 5

Simulations and Experiments

5.1 Measurement of disturbances

The disturbance acting on cleaning unit is originated from two main sources, the variation in distance between robot platform and wall and repetitive reaction from cleaning task. To estimate the magnitude and frequency response of disturbance, the experiment is executed on actual condition.

5.1.1 Disturbance from external wall and robotic platform

The experiment is experiment performed on the building of Institute of Advanced Machines and Design in Seoul National University, to measure the disturbance from robot platform. The Fig. 5. 1 Indicates the actual measurement in two different wall conditions.

Fig. 5. 1 Experiment of distance data between robot platform and wall of building

The velocity of robot platform is set to 9m/min and the obstacle with four different height, 15, 30, 40 and 110mm is used. The distance data measured twice during ascending and descending are indicated in Fig. 5. 2 below.

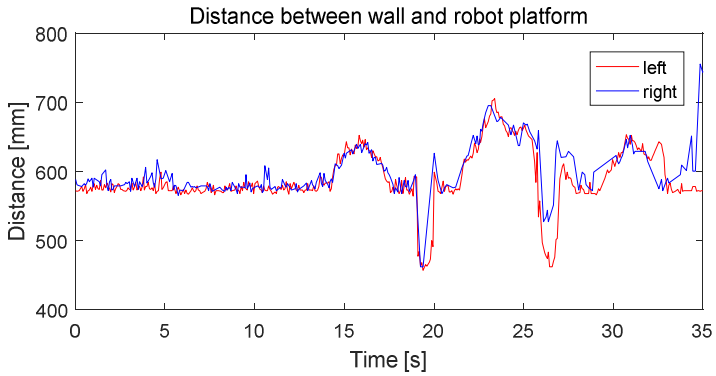

Fig. 5. 2 Distance data between robot platform and wall of building

Applying the fast fourier transform on the disturbance dataset measured during ascending and descending on each wall gives the following results in Fig. 5. 3 and Fig. 5.4.

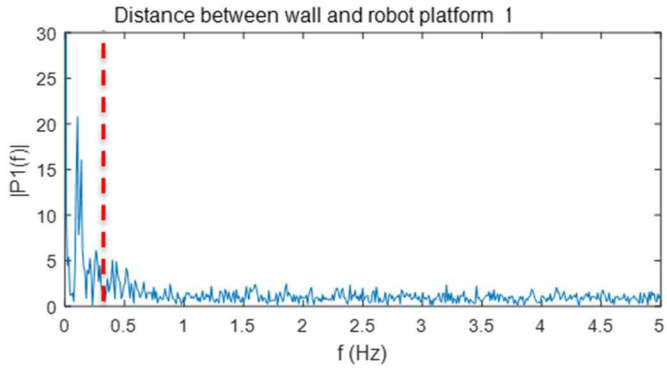

Fig. 5. 3 FFT data from distance data between robot platform and wall of building 1

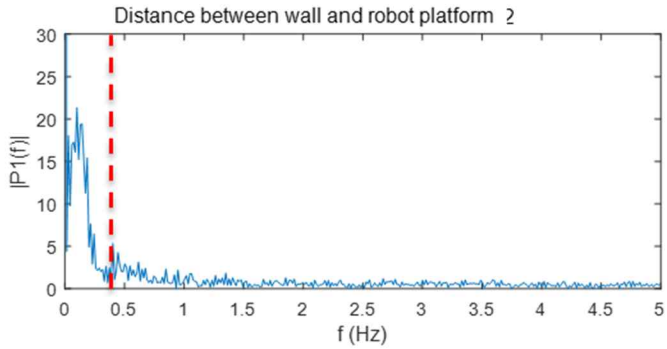

Fig. 5. 4 FFT data from distance data between robot platform and wall of building 2

As shown in the figure above, more than 90% disturbance is distributed below the 0.4Hz and the applicable maximum magnitude of disturbance is the 100mm, the limit of the adjusting mechanism in robot platform.

5.1.2 Disturbance from cleaning unit

The wall cleaning unit can be easily attached and detached to the robot platform with modular design and replacement of cleaning brush is possible. While cleaning the wall with rotating brush, the disturbance is originated from eccentricity, density and pattern of brush.

Fig. 5. 5 Experimental setup for measurement of cleaning unit disturbance

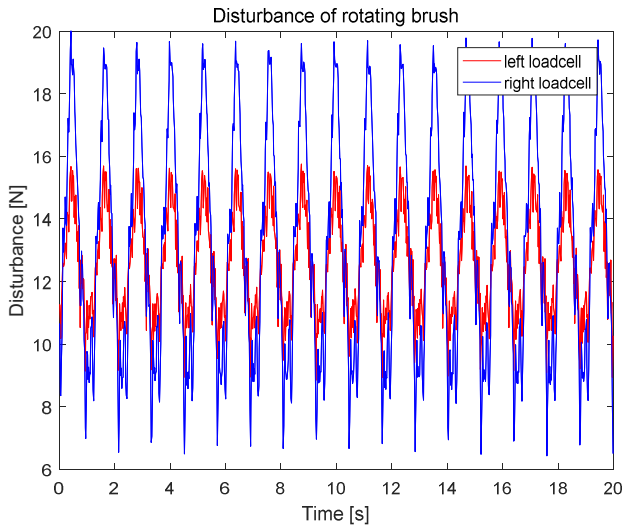

Fig. 5. 6 Disturbance data of rotating general type brush

The disturbance measured at both of load cell embedded on left and right side while rotating general type brush at 100RPM is indicated in Fig. 5. 6. As shown in the figure above, the frequency response is almost same in both of side whereas the magnitude is different from each other. The disturbance measured from each of brush are attached in below.

Table 5. 1 FFT data of disturbance measured from each of brush

 General type brush	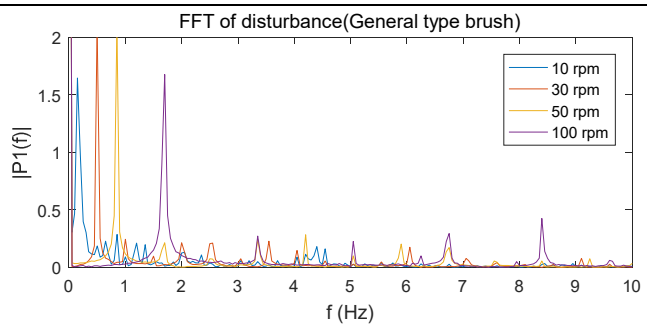 Disturbance from eccentricity : 5 – 14 N
 Spiral type brush	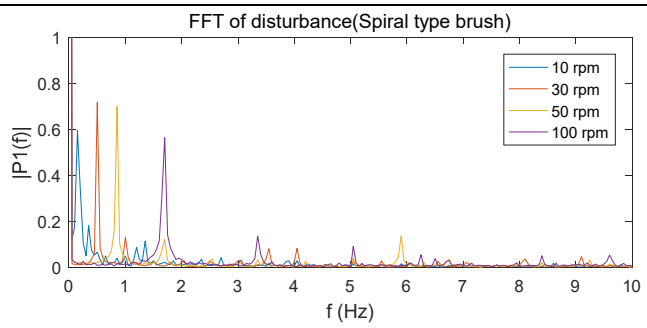 Disturbance from eccentricity : 3 – 6 N
 V-type brush	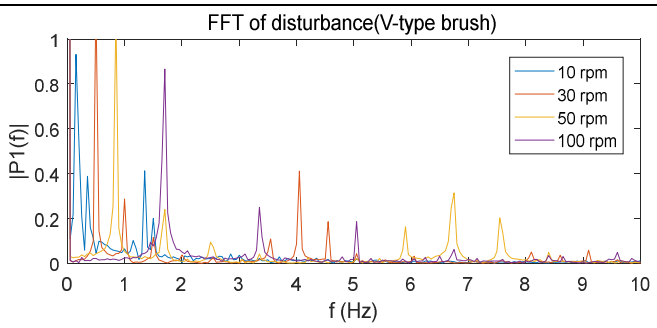 Disturbance from eccentricity : 4 – 8 N

The frequency response of disturbance from each brush follows the rotating RPM but the magnitude of the disturbance is different from the density and pattern of brush. Based on the data from the test, the controller on the test bench is constructed and performance test is executed.

5.2 Simulations

Tracking response of commanded force with applying position-based force tracking impedance control to two given disturbance input, step and sinusoidal wave, is indicated in Fig. 5. 7, Fig. 5. 8 and Fig. 5. 9. ($M = 1, B = 50, K = 100, k_p = 20, k_d = 0.01, k_i = 10, \eta = 10$)

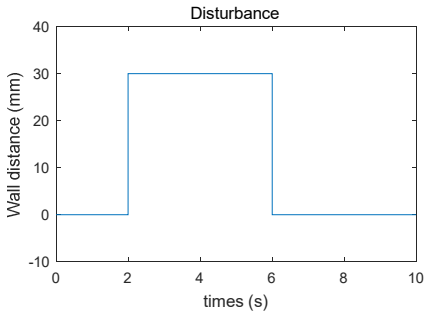

Fig. 5. 7 Disturbance of 30 mm, step

Table 5. 2 Control performance of each controller (30 mm, step)

FTIC	FTIC + DOB	FTIC + DOB + SMC
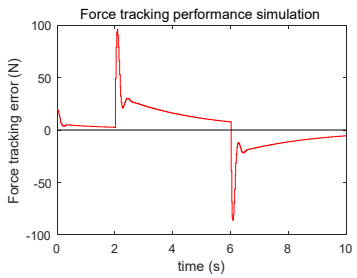	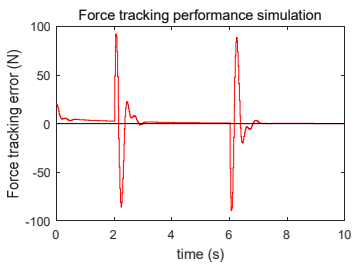	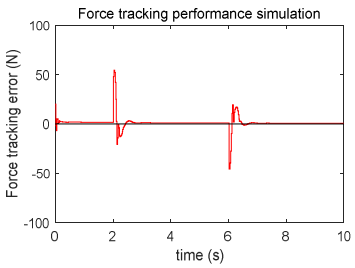
Max – Min : 182.35, STD : 18.76	Max – Min : 181.06, STD : 17.29	Max – Min : 100.24, STD : 6.51

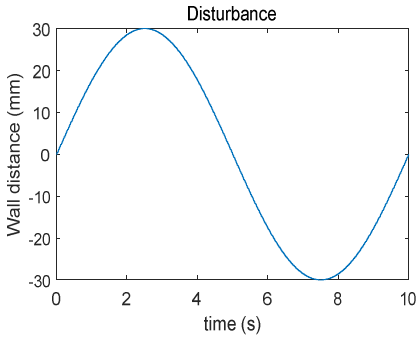

Fig. 5. 8 Disturbance of 0.1 Hz sinusoidal, 30 mm

Table 5. 3 Control performance of each controller (0.1 Hz, 30 mm sinusoidal)

FTIC	FTIC + DOB	FTIC + DOB + SMC
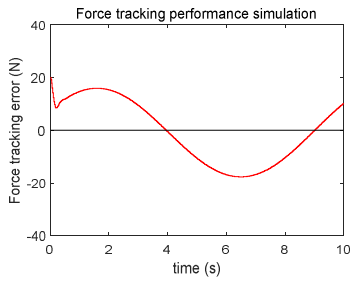	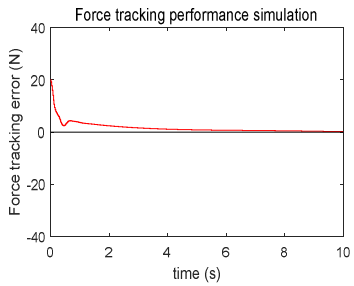	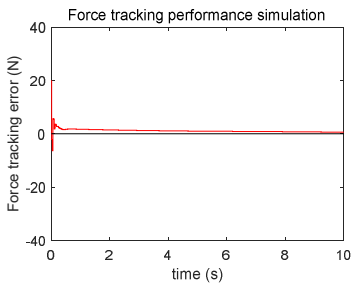
Max – Min : 37.66, STD : 11.95	Max – Min : 4.33, STD : 2.18	Max – Min : 3.67, STD : 1.04

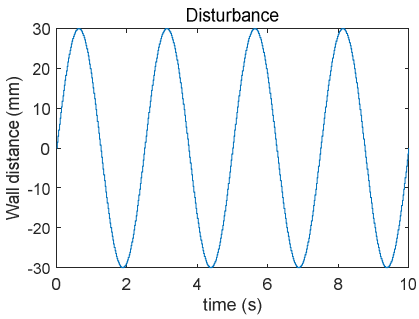

Fig. 5. 9 Disturbance of 0.4 Hz sinusoidal, 30 mm

Table 5. 4 Control performance of each controller (0.4 Hz, 30 mm sinusoidal)

FTIC	FTIC + DOB	FTIC + DOB + SMC
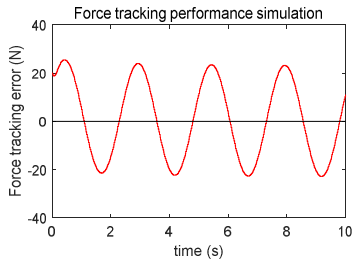	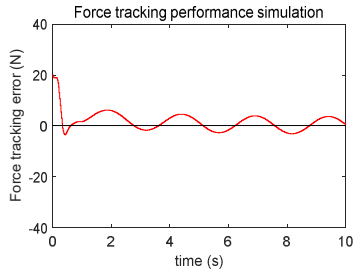	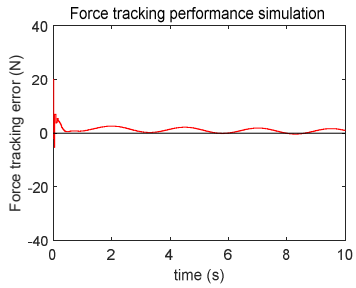
Max – Min : 48.43, STD : 16.50	Max – Min : 6.80, STD : 3.66	Max – Min : 2.29, STD : 1.32

Table 5. 5 Comparison of force tracking performance of each controller

Disturbance	FTIC		FTIC + DOB		FTIC + DOB + SMC	
	Max-Min	STD	Max-Min	STD	Max-Min	STD
Step	182.35	18.76	181.06	17.29	100.224	6.51
0.1 Hz	37.66	11.95	4.33	2.18	3.67	1.04
0.4 Hz	48.43	16.50	6.80	3.66	2.29	1.32

The above simulation results show that the disturbance of 0.1 Hz can remove more than 80% disturbance using disturbance observer. On the other hand, for the step and 0.4 Hz disturbance, the controller applying the sliding mode control has better disturbance compensation performance than the controller applied to the disturbance observer only by 60%.

The simulation for tracking response of commanded force is performed with the two given disturbance conditions for distance and brush. The variation of distance between wall and wall cleaning unit modeled with step and sinusoidal wave function and rotating speed of brush set to 100RPM is reflected on the simulation. The simulation results for each controller is shown in below.

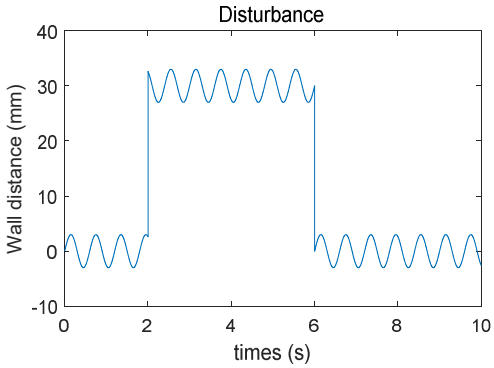

Fig. 5. 10 Disturbance of 30 mm, step and 100rpm, 3 mm sinusoidal

Table 5. 6 Control performance of each controller (30 mm, step and 100rpm, 3 mm sinusoidal)

FTIC	FTIC + DOB	FTIC + DOB + SMC
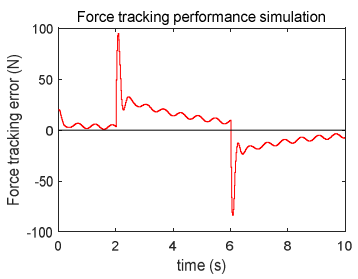	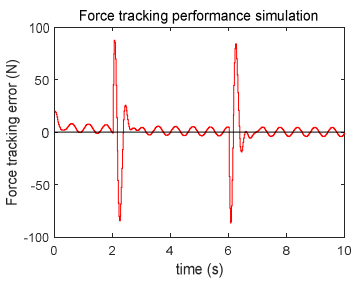	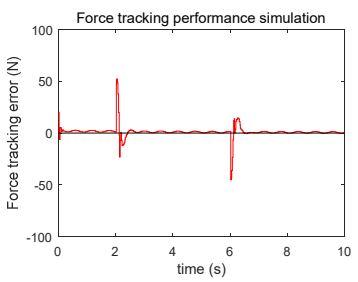
Max – Min : 178.51, STD : 18.65	Max – Min : 174.36, STD : 16.87	Max – Min : 96.95, STD : 6.07

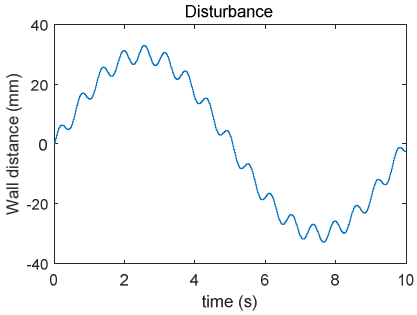

Fig. 5. 11 Disturbance of 0.1 Hz, 30 mm sinusoidal and 100 rpm, 3 mm sinusoidal

Table 5. 7 Control performance of each controller (0.1 Hz, 30 mm sinusoidal and 100 rpm, 3 mm sinusoidal)

FTIC	FTIC + DOB	FTIC + DOB + SMC
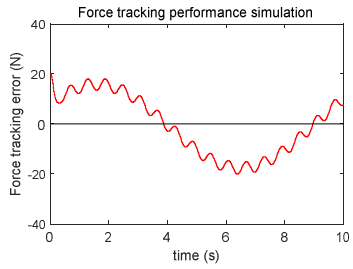	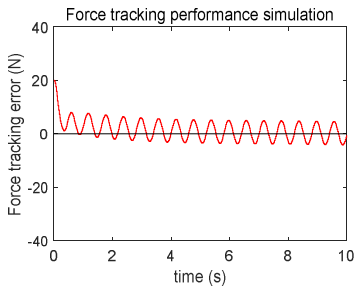	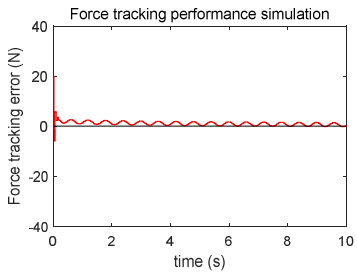
Max – Min : 40.05, STD : 12.07	Max – Min : 8.68, STD : 3.78	Max – Min : 6.05, STD : 1.19

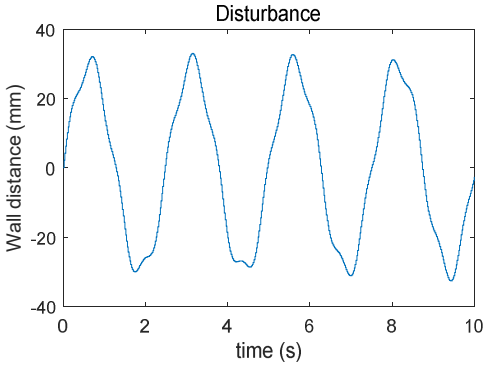

Fig. 5. 12 Disturbance of 0.4 Hz, 30 mm sinusoidal and 100 rpm, 3 mm sinusoidal

Table 5. 8 Control performance of each controller (0.4 Hz, 30 mm sinusoidal and 100 rpm, 3 mm sinusoidal)

FTIC	FTIC + DOB	FTIC + DOB + SMC
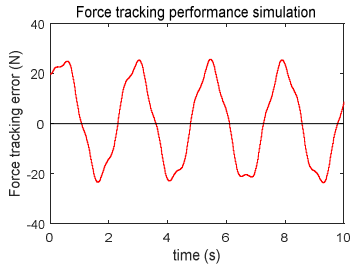	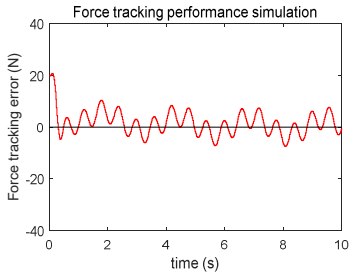	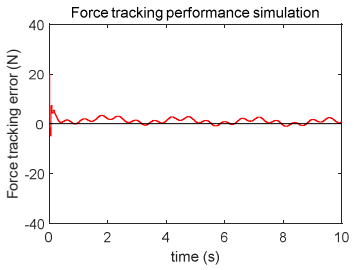
Max – Min : 49.36, STD : 16.57	Max – Min : 15.15, STD : 4.78	Max – Min : 6.05, STD : 1.43

Table 5. 9 Control performance of each controller (0.4 Hz, 30 mm sinusoidal and 100 rpm, 3 mm sinusoidal)

Disturbance	FTIC		FTIC + DOB		FTIC + DOB + SMC	
	Max-Min	STD	Max-Min	STD	Max-Min	STD
Step	178.51	18.65	174.36	16.87	96.95	6.07
0.1 Hz	40.05	12.07	8.68	3.78	6.05	1.19
0.4 Hz	49.36	16.57	15.15	4.78	6.05	1.43

For disturbances of 0.1 Hz and 0.4 Hz, the disturbance observer can reduce more than 60 % of the standard deviation of external disturbance. However, we could only reduce 10 % in case of step disturbance. On the other hand, applying the sliding mode control was more than 60% better than the disturbance observer.

5.3 Experiments

The test bench with 2 DOF on Fig. 5. 13(a) is designed to give the disturbance originated from the distance and angle between robot platform and wall as intended. The rotation about Z axis and translation along Y axis can be modified as shown below. Reflecting the mechanism of robot platform, it's also designed to move along vertically. The designed test bench is indicated in Fig. 5. 13(b).

(a)

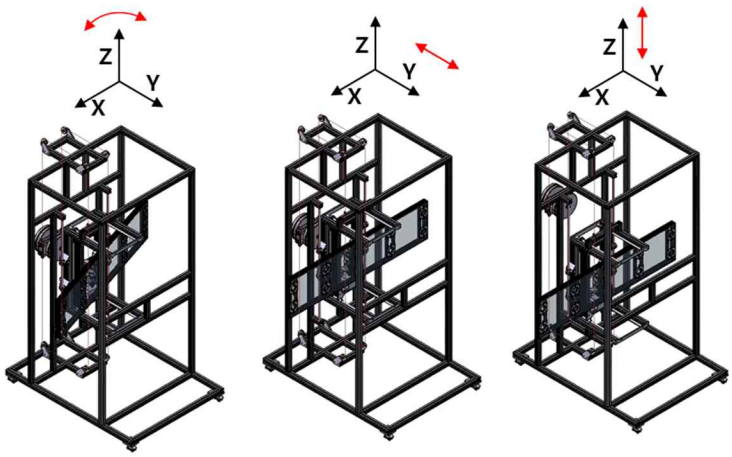

(b)

Fig. 5. 13 Test bench for evaluating the control performance of the cleaning unit

The experimental results when general type brush is applied with two sinusoidal waves disturbance which has same magnitude, 30mm, but different frequency, 0.1Hz and 0.4Hz is shown in below.

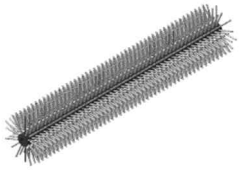

Fig. 5. 14 General type brush

(a)

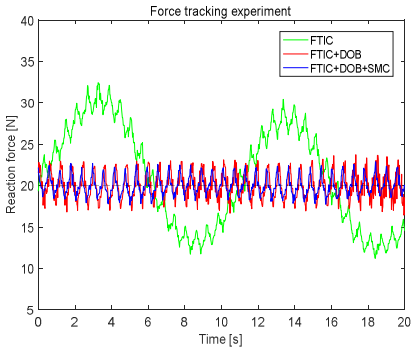

	FTIC	+DOB	+SMC
Standard deviation	6.04	1.63	1.13
Maximum difference	21.2	7.3	5.2

(b)

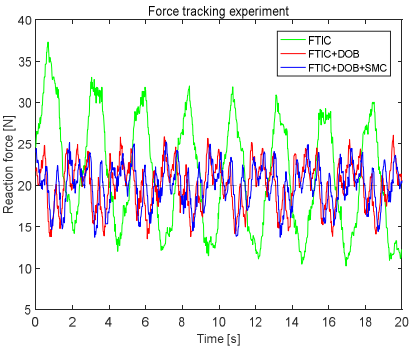

	FTIC	+DOB	+SMC
Standard deviation	6.69	2.81	2.32
Maximum difference	27.1	13.8	11.7

Fig. 5. 15 Experimental results of control performance at (a) 0.1 Hz, 30 mm (b) 0.4 Hz, 30 mm sinusoidal disturbance (General type brush)

The experimental results when spiral type brush is applied with two sinusoidal waves disturbance which has same magnitude, 30mm, but different frequency, 0.1Hz and 0.4Hz is shown in below

Fig. 5. 16 Spiral type brush

(a)

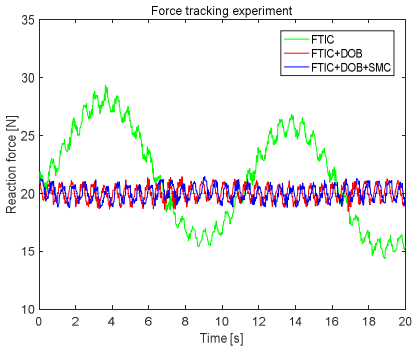

	FTIC	+DOB	+SMC
Standard deviation	4.13	0.65	0.64
Maximum difference	15.0	3.0	2.7

(b)

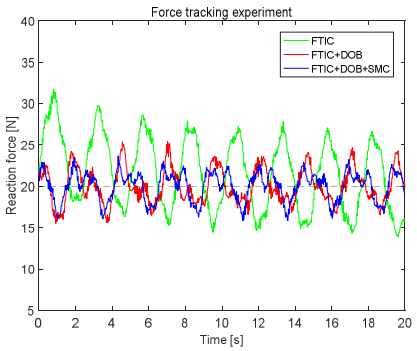

	FTIC	+DOB	+SMC
Standard deviation	4.34	2.01	1.77
Maximum difference	17.8	9.8	7.8

Fig. 5. 17 Experimental results of control performance at (a) 0.1 Hz, 30 mm (b) 0.4 Hz, 30 mm sinusoidal disturbance (Spiral type brush)

The experimental results when V-type brush is applied with two sinusoidal waves disturbance which has same magnitude, 30mm, but different frequency, 0.1Hz and 0.4Hz is shown in below

Fig. 5. 18 V-type brush

(a)

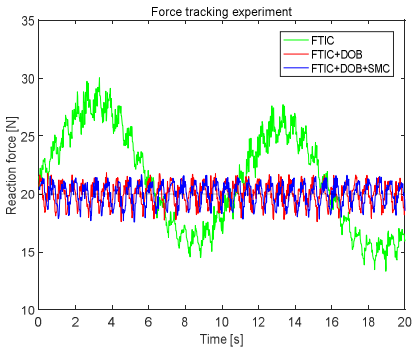

	FTIC	+DOB	+SMC
Standard deviation	4.27	0.94	0.91
Maximum difference	16.7	4.2	4.1

(b)

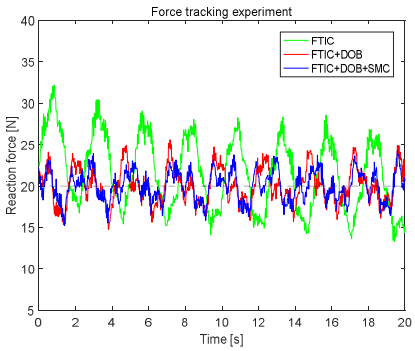

	FTIC	+DOB	+SMC
Standard deviation	4.34	2.17	1.78
Maximum difference	18.9	10.8	9.0

Fig. 5. 19 Experimental results of control performance at (a) 0.1 Hz, 30 mm (b) 0.4 Hz, 30 mm sinusoidal disturbance (V-type brush)

Table 5. 10 Experimental data of control performance of each controller

Disturbance	Type of brush	FTIC		FTIC + DOB		FTIC + DOB + SMC	
		Max-Min	STD	Max-Min	STD	Max-Min	STD
0.1 Hz	General	21.2	6.04	7.3	1.63	5.2	1.13
	Spiral	15.0	4.13	3.0	0.65	2.7	0.64
	V	16.7	4.27	4.2	0.94	4.1	0.91
0.4 Hz	General	27.1	6.69	13.8	2.81	11.7	2.32
	Spiral	17.8	4.34	9.8	2.01	7.8	1.77
	V	18.9	4.34	10.8	2.17	9.0	1.78

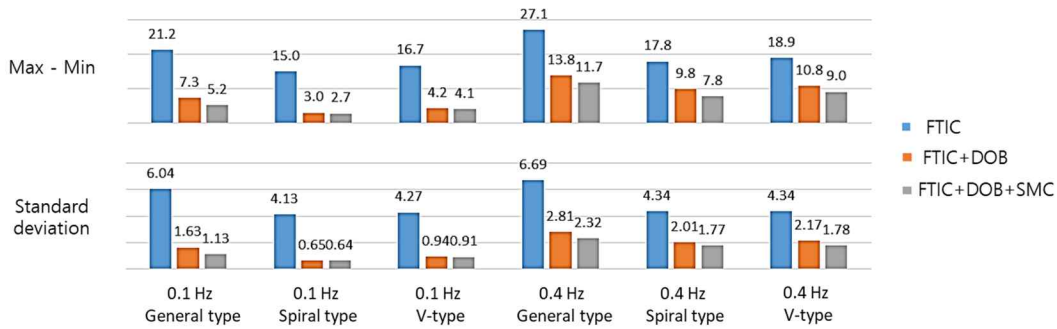

Fig. 5. 20 Comparison of control performance of each controller

Experimental results show that the addition of disturbance observer reduces the maximum difference by 58 % and the standard deviation by 66 %, compared to using only position-based force tracking impedance control. The controller with sliding mode control showed 65 % and 71 % of disturbance reduction, respectively. Therefore, the overall control system satisfies the desired performance and stability condition

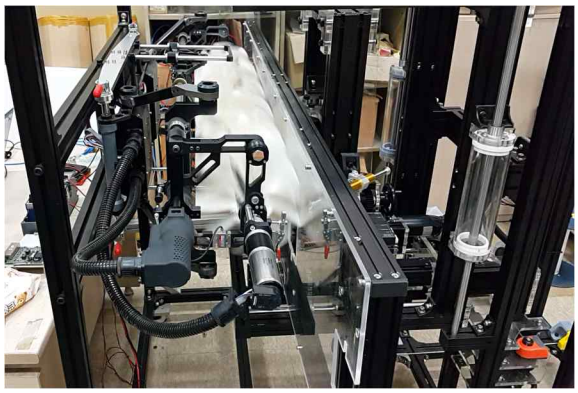

Fig. 5. 21 Force control experiment of cleaning unit

The experimental results when rotating brush is applied with step disturbance of 50 mm is shown in Fig. 5. 22.

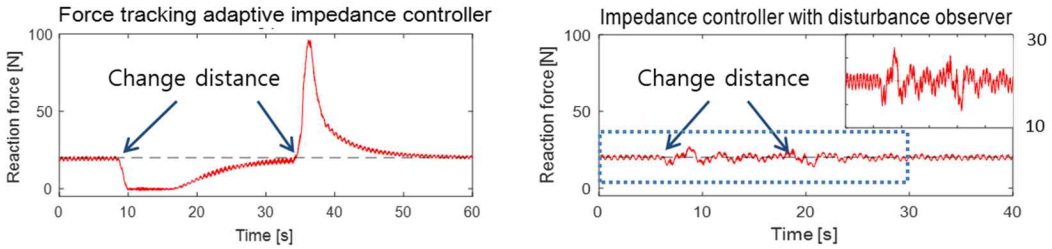

Fig. 5. 22 Experimental results of control performance at step disturbance of 50 mm

Table 5. 11 Comparison of control performance at step disturbance of 50 mm

Without Disturbance observer		With Disturbance observer	
Max-Min	Standard deviation	Max-Min	Standard deviation
97.5	15.7	13.6 (▼86 %)	1.8 (▼89 %)

The experimental results when rotating brush is applied with angle disturbance of $\pm 3.5°$ between the cleaning unit and the wall is shown in Fig. 5. 23.

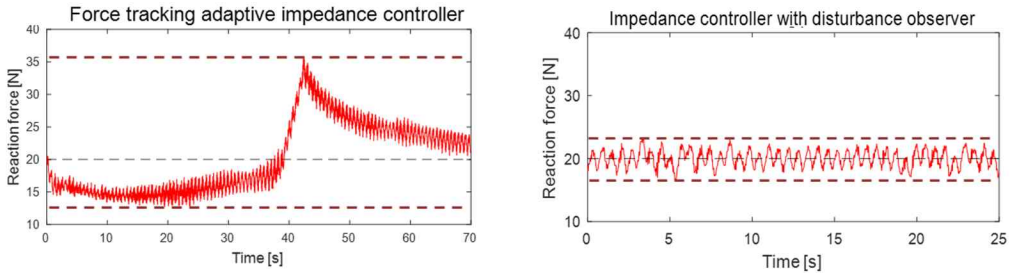

Fig. 5.23 Experimental results of control performance at angle disturbance of $\pm 3.5°$

Table 5. 12 Comparison of control performance at angle disturbance of $\pm 3.5°$

Without Disturbance observer		With Disturbance observer	
Max-Min	Standard deviation	Max-Min	Standard deviation
23.1	5.5	6.8 (▼71 %)	1.3 (▼76 %)

Chapter 6

Conclusion

In this paper, the modular wall cleaning unit which can be attached and detached from the wall climbing robot platform is designed and proposed. The wall cleaning unit can also change the brushes with different density and pattern suitable for target wall easily and is constructed with modular design for this. The brush cleans the wall through friction originating from rotation of it. For optimization of cleaning performance, Taguchi Method is used for selecting optimized using condition.

To guarantee cleaning performance, it's most important to maintain contact force within certain level. However, it's hard to construct the dynamic model due to the compliance originated coupling used for connection with robot platform and brush. To overcome this, adaptation law is added to position-based impedance control and makes commanded force tracking possible

The algorithm for compensating the disturbance from both of the distance variation between wall and wall cleaning unit and brush rotation is designed and the nonlinearity originated from brush is reflected in it. With the disturbance observer, the disturbance existed in the model is eliminated and sliding mode control is added for removing the non-modeled

disturbance.

First of all, the interaction model between cleaning unit and wall is identified with system identification and Q-filter is designed with considering uncertainty in model parameters. The stability of disturbance observer is verified. Secondly, the stability for overall system combining both of the position-based force tracking impedance control and disturbance observer is verified. Finally, sliding surface is designed and the stability condition with all of the control input is proven.

The disturbance originated from robot platform and cleaning unit is measured to remake the actual field condition and this is reflected in the test bench design. The performance and stability of the proposed controller is verified with the simulation and experiment.

Bibliography

[1] F.W. Bach, M. Rachkov, J. Seevers, et al., “High tractive power wall-climbing robot”, Automation in Construction, vol. 4, pp. 213-224, 1995.

[2] A. Brunete, M. Hernando, J.E. Torres, et al., “Heterogeneous multi-configurable chained microrobot for the exploration of small cavities”, Automation in Construction, vol. 21, pp. 184-198, 2012.

[3] F. Cepolina, R. Michelini, R. Razzoli, et al., “Gecko, a climbing robot for wall cleaning”, 1st International Workshop on Advances in Service Robotics, Bardolino, Italy, 2003.

[4] H. Kim, D. Kim, H. Yang, et al., “Development of a wall-climbing robot using a tracked wheel mechanism”, Journal of Mechanical Science and Technology, vol. 22, pp. 1490-1498, 2008.

[5] M.F. Silva, J.A. Machado, J.K. Tar, “A survey of technologies for climbing robots adhesion to surfaces”, IEEE 6th International Conference On Computational Cybernetics, Stara Lesna, Slovakia, 2008, pp. 127-132.

[6] B. Chu, K. Jung, C. Han, D. Hong, “A survey of climbing robots: locomotion and adhesion”, International Journal of Precision Engineering and Manufacturing, vol. 11, isuue. 4, pp. 633-647, 2010.

[7] E. Gambao, M. Hernando, “Control System for a semi-automatic façade cleaning robot”, Proceedings of the 23rd ISARC, Tokyo, Japan, 2006, pp.406-411.

[8] T. Akinfiev, M. Armada, S. Nabulsi, “Climbing cleaning robot for vertical surfaces”, Industrial Robot: An International Journal, vol. 36, pp. 352-357, 2009.

[9] N. Elkmann, D. Kunst, T. Krueger, et al., “SIRIUSc – façade cleaning robot for a high-rise building in Munich, Germany”, Proceedings of the 7th International Conference on Climbing and Walking Robots, Madrid, Spain, 2004, pp.1033-1040.

[10] H. Zhang, F. Zhang, W. Wang, et al., “A series of pneumatic glass-wall cleaning robots for high-rise buildings”, Industrial Robot: An International Journal, vol. 34/2, pp. 150-160, 2007.

[11] S. Moon, J. Huh, D. Hong, et al., “Vertical motion control of building facade maintenance robot with built-in guide rail”, Robotics and Computer-Integrated Manufacturing, vol. 31, pp. 11-20, 2015.

[12] S. Moon, J. Huh, K.W. Oh, et al., “Window cleaning system with water circulation for building facade maintenance robot and its efficiency analysis”, International Journal of Precision Engineering and Manufacturing-Green Technology, vol. 2, pp. 65-72, 2015.

[13] D. Schmidt, K. Berns, “Climbing robots for maintenance and inspections of vertical structures-A survey of design aspects and technologies”, Robotics and Autonomous Systems, vol. 61, pp. 1288-1305, 2013.

[14] K. Seo, S. Cho, T. Kim, H.S. Kim, et al., “Design and stability analysis of a novel wall-climbing robotic platform (ROPE RIDE)”, Mechanism and Machine Theory Vol. 70, pp. 189-208, 2013.

[15] T. Kim, H.S. Kim, J. Kim, “Position-based impedance control for force tracking of a wall-cleaning unit”, International Journal of Precision Engineering and Manufacturing Vol. 17/3, pp. 323-329, 2016.

[16] H. Sadjadian, H. D. Taghirad, “Comparison of different methods for computing the forward kinematics of a redundant paraller manipulator”, Journal of Intelligent and Robotic Systems, pp. 225-246, 2005.

[17] N. Hogan, “Impedance control:. An approach to manipulation”, American Control Conference, 1984, pp.303-313.

[18] X. Chen, T. Fukuda, K. D. Young, “A new nonlinear robust disturbance observer” Systems & control Letters, Vol. 41, Issue. 3, pp.189-199, 2000.

[19] J. Han, “From PID to active disturbance rejection control”, IEEE Transactions on Industrial Electronics, Vol 56, No. 3, pp. 900-906, 2009.

[20] C. C. Wang, M. Tomizuka, “Design of robustly stable disturbance observers based on closed loop consideration using H_∞ optimization and its applications”, Proceeding of the American Control Conference, Boston, Massachusetts, 2004, pp. 3764-3769.

[21] H. H. Choi, “LMI-based sliding surface design for integral sliding model control of mismatched uncertain systems”, IEEE Transactions on Automatic Control, Vol. 52, No. 4, pp.736-742, 2007.

[22] Q. Xu, “Adaptive discrete-time sliding mode impedance control of a piezoelectric microgripper”, IEEE Transactions on Robotics, Vol.29, No. 3, pp.663-673, 2013.

Abstract in Korean

고층빌딩은 점차 높아지고 있고 그 수가 증가하고 있지만 건물 유지보수를 위해 필요한 외벽 청소는 작업자의 수작업에 의존하고 있다. 작업자는 위험에 항상 노출되어 있으며 매년 인명피해가 발생하고 있다. 따라서 작업자의 안전을 보장하고 작업의 효율성을 높이기 위해 외벽 청소 작업을 로봇으로 대체하고자 하는 연구가 꾸준히 이루어지고 있다.

본 논문은 다양한 외벽의 형상에 적용 가능하고 작업의 확장이 용이한 모듈형 구조의 외벽 청소 로봇을 제시한다. 등반 로봇 플랫폼은 외벽에 부착되어 등하강이 가능하며 모듈형 결합부를 통해 청소 유닛의 탈부착이 용이한 구조이다. 청소유닛은 건식 청소 유닛과 반습식 청소 유닛 두 가지가 개발되었으며 청소면의 종류, 오염도에 따라 교체하여 사용할 수 있다. 청소유닛은 볼스크류 매커니즘을 통해 등반 방향의 수직한 면으로 2 자유도의 움직임이 가능하며 벽면과의 거리나 각도가 달라질 때 적응이 가능하다. 청소유닛 작업영역의 양 끝에는 반력을 측정할 수 있는 센서가 장착되었으며 청소 성능을 일정하게 유지하기 위하여 반력을 일정하게 유지할 수 있는 힘 제어 알고리즘이 필수적이다.

청소유닛의 힘 제어는 위치 기반의 간접 제어 방식인 임피던스 제어 구조를 사용하여 구현하였다. 또한 전체 제어기는 힘 추종 임피던스 제어기에 외란 관측기와 슬라이딩 모드 제어기를 결합하였다. 제어기 목표는 등반 로봇 플랫폼과 벽면간의 거리 변화와 청소유닛 브러쉬의 회전으로 인해 생기는 외란, 시스템 파라미터의 오차로 인해 생기는 외란을 보상하는 것이다. 외란 관측기는 청소유닛과 주위 환경과의 상호작용 모델링을 기반으로 목표 힘과 실제 힘과의 차이에 대한 보상 입력을 도출하고 슬라이딩 모드 제어는 모델링 되지 않은 외

란에 대해서 보상하는 역할을 한다.

설계된 전체 제어기에 대해서 안정성을 해석하고 시뮬레이션을 통하여 설계한 제어기의 타당성을 검증한다. 실제 외벽에서의 작업을 재현하기 위한 테스트벤치를 제작하고 실제 청소유닛에 적용하여 실험을 수행함으로써 설계된 제어기의 외란 제거 성능을 확인하였다.

주요어 : 외벽 청소 로봇, 모듈형 매니퓰레이터, 임피던스 제어, 외란관측기, 슬라이딩 모드 제어

학번 : 2011-20700